Discovery, Biosynthesis and Stress-Related Accumulation of Dolabradiene-Derived Defenses in Maize[1[OPEN]]

Sibongile Mafu,[a,2,3] Yezhang Ding,[b,2] Katherine M. Murphy,[a] Omar Yaacoobi,[a] J. Bennett Addison,[c] Qiang Wang,[d] Zhouxin Shen,[b] Steven P. Briggs,[b] Jörg Bohlmann,[e] Gabriel Castro-Falcon,[f] Chambers C. Hughes,[f] Mariam Betsiashvili,[b] Alisa Huffaker,[b] Eric A. Schmelz,[b] and Philipp Zerbe[a,4]

[a]Department of Plant Biology, University of California, Davis, California
[b]Section of Cell and Developmental Biology, University of California, La Jolla, California
[c]Department of Chemistry, San Diego State University, San Diego, California
[d]College of Agronomy and Institute of Ecological Agriculture, Sichuan Agricultural University, Chengdu 611130, China
[e]Michael Smith Laboratories, University of British Columbia, Vancouver, British Columbia, Canada V6T 1Z4
[f]Center for Marine Biotechnology and Biomedicine, Scripps Institution of Oceanography, University of California, La Jolla, California

ORCID IDs: 0000-0001-5903-1870 (Y.D.); 0000-0002-8891-4274 (K.M.M.); 0000-0002-3683-3245 (O.Y.); 0000-0002-7487-4064 (Z.S.); 0000-0002-7226-8618 (S.P.B.); 0000-0002-3637-7956 (J.B.); 0000-0002-3504-0980 (G.C.-F.); 0000-0002-3886-8433 (A.H.); 0000-0002-2837-734X (E.A.S.); 0000-0001-5163-9523 (P.Z.).

Terpenoids are a major component of maize (*Zea mays*) chemical defenses that mediate responses to herbivores, pathogens, and other environmental challenges. Here, we describe the biosynthesis and elicited production of a class of maize diterpenoids, named dolabralexins. Dolabralexin biosynthesis involves the sequential activity of two diterpene synthases, *ENT*-COPALYL DIPHOSPHATE SYNTHASE (ZmAN2) and KAURENE SYNTHASE-LIKE4 (ZmKSL4). Together, ZmAN2 and ZmKSL4 form the diterpene hydrocarbon dolabradiene. In addition, we biochemically characterized a cytochrome P450 monooxygenase, ZmCYP71Z16, which catalyzes the oxygenation of dolabradiene to yield the epoxides 15,16-epoxydolabrene (epoxydolabrene) and 3β-hydroxy-15,16-epoxydolabrene (epoxydolabranol). The absence of dolabradiene and epoxydolabranol in *Zman2* mutants under elicited conditions confirmed the in vivo biosynthetic requirement of ZmAN2. Combined mass spectrometry and NMR experiments demonstrated that much of the epoxydolabranol is further converted into 3β,15,16-trihydroxydolabrene (trihydroxydolabrene). Metabolite profiling of field-grown maize root tissues indicated that dolabralexin biosynthesis is widespread across common maize cultivars, with trihydroxydolabrene as the predominant diterpenoid. Oxidative stress induced dolabralexin accumulation and transcript expression of *ZmAN2* and *ZmKSL4* in root tissues, and metabolite and transcript accumulation were up-regulated in response to elicitation with the fungal pathogens *Fusarium verticillioides* and *Fusarium graminearum*. Consistently, epoxydolabranol significantly inhibited the growth of both pathogens in vitro at 10 μg mL^{-1}, while trihydroxydolabrene-mediated inhibition was specific to *F. verticillioides*. These findings suggest that dolabralexins have defense-related roles in maize stress interactions and expand the known chemical space of diterpenoid defenses as genetic targets for understanding and ultimately improving maize resilience.

Plants produce diverse arrays of specialized metabolites that govern interactions with, and adaptation to, their biotic and abiotic environments (Pichersky and Gershenzon, 2002; Hartmann, 2007; Pichersky and Lewinsohn, 2011; Tholl, 2015). Among these specialized metabolites, diterpenoids are a large class of more than 10,000 known compounds with diverse physiological and biological functions. Plants typically harbor both a widely conserved subset of diterpenoids such as the GAs, a class of phytohormones mediating developmental processes, and myriad specialized compounds with diverse roles in chemical ecology and plant adaptation (Keeling and Bohlmann, 2006; Gershenzon and Dudareva, 2007; Chaturvedi et al., 2012; Schmelz et al., 2014; Hedden and Sponsel, 2015). Because of their agronomic importance as two of the world's major food crops, maize (*Zea mays*) and rice (*Oryza sativa*) have been studied extensively for their terpenoid-based defense systems (Degenhardt, 2009; Schmelz et al., 2014). In rice, a suite of momilactone, oryzalexin, and phytocassane diterpenoids confer defense against several major pathogens, such as rice blast (*Magnaporthe oryzae*; Peters, 2006; Kato-Noguchi and Kobayashi, 2009; Toyomasu et al., 2014). As components of rice root exudates, momilactones also can exhibit allelopathic activity, suppressing the development of neighboring plants of other species (Kato-Noguchi and Peters, 2013). These findings exemplify the diverse, protective biological roles of diterpenoids in Poaceae crops. However, the potential applications of these chemical defenses in agricultural improvement have been limited, in part, by knowledge gaps in understanding identities, biosynthesis, regulation, and ecological roles in different crop species.

In maize, two groups of acidic terpenoids, the kauralexin class of diterpenoids and the zealexin class of

sesquiterpenoids (Fig. 1), are part of a complex repertoire of defense-related specialized metabolites, such as phenylpropanoids, oxylipins, benzoxazinoids, and volatile terpenoids (Schnee et al., 2006; Köllner et al., 2008a; Santiago and Malvar, 2010; Ahmad et al., 2011; Huffaker et al., 2011; Schmelz et al., 2011; Christensen et al., 2015; Richter et al., 2016; Wouters et al., 2016). Inducible zealexin and kauralexin production contributes to defense, both aboveground and belowground, against pathogenic fungi, including *Fusarium*, *Aspergillus*, and *Colletotrichum* spp. (Huffaker et al., 2011; Schmelz et al., 2011; Vaughan et al., 2015). Kauralexins also function as insect feeding deterrents (Schmelz et al., 2011) and accumulate in response to salt and drought stress (Vaughan et al., 2015). These properties are consistent with diverse roles in stress resilience that extend well beyond antimicrobial activity.

Much of the diterpenoid chemical diversity of plants is produced through the sequential activity of enzymes encoded by two functionally diverse gene families, the diterpene synthases (diTPSs) and the cytochrome P450 monooxygenases (P450s). Plants employ variable combinations of different diTPSs and P450s to transform a few ubiquitous diterpene precursors into thousands of different diterpenoid metabolites, many of which are of limited taxonomic distribution (Peters, 2010; Zerbe and Bohlmann, 2015). Modular enzyme networks largely determine the variations of diterpene profiles in closely and distantly related plant species (Peters, 2010; Hamberger and Bak, 2013; Zerbe and Bohlmann, 2015). Naturally occurring modularity in diterpenoid biosynthesis further enables the engineering of combinatorial diTPS and P450 expression systems in microbial and plant host systems to accelerate the discovery of terpenoid pathways (Brückner and Tissier, 2013; Lange and Ahkami, 2013; Kitaoka et al., 2015; Zerbe and Bohlmann, 2015).

In monocots, diterpenoid pathway networks comprise sets of diTPSs with conserved and species-specific functions in wheat (*Triticum aestivum*) and rice (Prisic et al., 2004; Xu et al., 2004, 2007a; Morrone et al., 2006; Wu et al., 2012; Zhou et al., 2012; Fu et al., 2016). The ensuing diTPS products often undergo further structural modifications through the activity of P450 enzymes, as exemplified in rice by the P450-catalyzed formation of several bioactive diterpenoid metabolites (Swaminathan et al., 2009; Wang et al., 2011, 2012a, 2012b). Comparatively, less was known about the complexity of maize diterpenoid biosynthesis. Characterized maize diterpenoid enzymes include the *ENT*-COPALYL DIPHOSPHATE (CPP) SYNTHASE ZmAN1 (Bensen et al., 1995), the *ENT*-KAURENE SYNTHASES ZmTPS1, ZmKLS3, and ZmKSL5 (Fu et al., 2016), and the *ENT*-KAURENE OXIDASE CYP701A26 (Mao et al., 2017; Fig. 1). All of these enzymes have either validated or predicted roles in GA metabolism. However, the frequently observed substrate promiscuity of characterized enzymes (Peters, 2010; Morrone et al., 2011; Zerbe and Bohlmann, 2015) also may enable roles in defense-related specialized metabolism. In the absence of mutant analyses, the maize kauralexin and zealexin metabolic pathways have remained largely unproven, with the exception of the *ent*-CPP synthase ZmAN2, which has been empirically demonstrated to function in kauralexin formation (Harris et al., 2005; Vaughan et al., 2015). The β-macrocarpene synthases ZmTPS6, ZmTPS11, and ZmCYP71Z18 have been assigned to the zealexin pathway based on predictions from in vivo biochemical assays (Köllner et al., 2008b; Mao et al., 2016).

In this study, we functionally characterized ZmAN2, ZmKSL4, and ZmCYP71Z16, which together form a biosynthetic branch of diterpenoids, termed dolabralexins. Patterns of inducible dolabralexin accumulation and gene expression in maize roots exposed to different stresses, combined with the antifungal bioactivity of 3β-hydroxy-15,16-epoxydolabrene (epoxydolabranol) and 3β,15,16-trihydroxydolabrene (trihydroxydolabrene), support diverse roles for dolabralexins in the maize defensive arsenal.

RESULTS

The Maize Diterpene Synthase Family

The maize genome sequence (B73 RefGen_v3) encodes a group of four class II diTPSs (ZmAN1, ZmAN2, ZmCPS3, and ZmCPS4) and six class I diTPSs (ZmTPS1 and ZmKSL1–ZmKSL5). Of the identified class I diTPSs, three (ZmTPS1, ZmKSL3, and ZmKSL5) have been characterized as *ent*-kaurene synthases (Fu et al., 2016) and three members (ZmKSL1, ZmKLS2, and

[1] P.Z. gratefully acknowledges support by startup funds through the University of California Davis and the Hellman Foundation, J.B. acknowledges support from the Natural Sciences and Engineering Research Council (NSERC) of Canada, E.A.S. and A.H. acknowledge primary support from the University of California San Diego startup funds and partial support for this work through a NSF-IOS Competitive Award (#1139329). P.Z., E.A.S., and A.H. collectively acknowledge support from the DOE Joint Genome Institute Community Science Program (grant #WIP 2568).

[2] These authors contributed equally to the article.

[3] Current address: University of Massachusetts, Department of Biochemistry and Molecular Biology, Life Science Laboratories, Amherst, MA 01003.

[4] Address correspondence to pzerbe@ucdavis.edu.

The author responsible for distribution of materials integral to the findings presented in this article in accordance with the policy described in the Instructions for Authors (www.plantphysiol.org) is: Philipp Zerbe (pzerbe@ucdavis.edu).

P.Z., E.A.S., A.H., and J.B. conceived the original research, designed the experiments, and oversaw data analysis; S.M., Y.D., and K.M.M. performed most experiments; O.Y., M.B., and E.A.S. assisted with diterpenoid metabolite purifications; J.B.A., G.C.-F., and C.C.H. assisted with NMR analyses of 3β,15,16-trihydroxydolabrene; Z.S. and S.P.B. assisted with high-mass-resolution MS/MS experiments; Q.W. contributed to enzyme analysis; P.Z. wrote the article with contributions of all the authors.

[OPEN] Articles can be viewed without a subscription.

www.plantphysiol.org/cgi/doi/10.1104/pp.17.01351

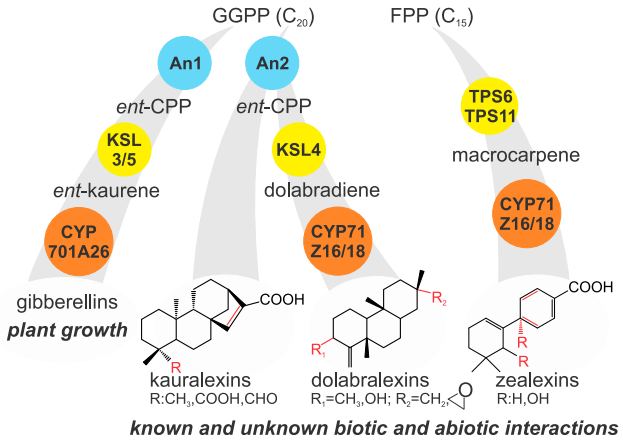

Figure 1. Modular systems of TPS and P450 enzymes in the biosynthesis of maize GAs, kauralexins, dolabralexins, and zealexins. Maize deploys functionally diverse class II diTPSs (blue), class I diTPSs (yellow), and P450 enzymes (orange) to form an array of biologically active terpenoid metabolites that function as GA phytohormones and in the response to both biotic and abiotic stress. The zealexin sesquiterpenoids and kauralexin diterpenoids were identified previously as components of the maize defense system (Huffaker et al., 2011; Schmelz et al., 2011). The stress-inducible dolabralexins represent an additional family of defense-related maize diterpenoids. Structural variations of the individual terpenoid groups are depicted as R. FPP, Farnesyl diphosphate; GGPP, geranylgeranyl diphosphate.

ZmKSL4) are of unknown function. Phylogenetic analysis placed ZmKSL1, ZmKLS2, and ZmKSL4 adjacent to rice diTPSs of specialized metabolism (Fig. 2). Most members of the maize diTPS gene family are dispersed across the genome (Supplemental Fig. S1), which differs from the clustering of genes of specialized diterpenoid pathways in rice (Schmelz et al., 2014). However, the maize *ent*-CPP synthases, ZmAN1, which functions in GA biosynthesis (Bensen et al., 1995), and ZmAN2, which has functions in specialized metabolism (Harris et al., 2005), colocalize with ZmKSL4 on chromosome 1, with distances of ~4 and ~159 Mb, respectively.

ZmKSL4 Produces an Unusual Diterpene Scaffold

To test for the activity of ZmKSL4 in specialized diterpenoid metabolism, we utilized the combinatorial functionality of class II and class I diTPSs of different plant species, which can be exploited to probe diTPS functions (Brückner and Tissier 2013; Zerbe et al., 2013; Kitaoka et al., 2015). An established *Escherichia coli* coexpression system (Morrone et al., 2010) was used to analyze the coupled activities of ZmKSL4 with (1) the *ent*-CPP synthase ZmAN2, (2) the rice *syn*-CPP synthase (OsCPS4; Xu et al., 2004), and (3) the grand fir (*Abies grandis*) abietadiene synthase variant D621A that produces CPP of normal [i.e. (+)] stereochemistry (Morrone et al., 2010). These three different combinations were selected, since *ent*-, *syn*-, and (+)-CPP represent the known stereochemical variations of class II diTPS products occurring naturally in many monocots (Peters, 2010; Schmelz et al., 2014). When coexpressed with ZmAN2, ZmKSL4 converted *ent*-CPP into a single product with an unusual fragmentation pattern showing major mass ions of mass-to-charge ratio (m/z) 204, 189, and 216, in addition to the mass ions m/z 257 and 272 that are characteristic of labdane diterpenoid structures (Fig. 2, compound **1**). Preparative enzymatic synthesis and purification of this product by silica chromatography and semipreparative HPLC enabled 1D and 2D NMR analyses and identified the ZmAN2/ZmKSL4 product as dolabradiene (Fig. 2; Supplemental Fig. S2). In addition, ZmKSL4 was active in combination with (+)-CPP to yield low amounts of several other diterpenoids (compounds **2**–**9**), of which (+)-pimara-8,15-diene **2** and (+)-sandaracopimaradiene **3** could be identified by comparison with authentic standards (Fig. 2; Supplemental Fig. S3). Similarly, ZmKLS4 showed activity with *syn*-CPP, resulting in the formation of *syn*-isopimara-7,15-diene **10**, *syn*-pimara-7,15-diene **11**, and *syn*-pimara-9(11),15-diene **12**.

ZmAN2, ZmKSL4, and ZmCYP71Z16 Function Together to Form 15,16-Epoxydolabrene

To gain insight into the structural elaboration of the predominant product of ZmAN2/ZmKSL4, namely dolabradiene, we tested its further modification by maize P450s. To this end, we performed a BLAST search of the B73 RefGen_v3 genome against monocot P450s of the CYP71, CYP76, and CYP99 families known to function in terpenoid metabolism. This search identified a member of the CYP71 family, ZmCYP71Z16, which showed high protein sequence similarity (89%) to the recently reported maize ZmCYP71Z18 involved in zealexin biosynthesis (Mao et al., 2016). Phylogenetic analysis placed ZmCYP71Z16 adjacent to ZmCYP71Z18 within a clade that also contained the rice P450s CYP71Z1, CYP71Z6, and CYP71Z7, of which CYP71Z6 and CYP71Z7 catalyze reactions in oryzalide and phytocassane biosynthesis (Wu et al., 2011; Fig. 3).

To biochemically characterize ZmCYP71Z16, a codon-optimized and N-terminally modified coding sequence was synthesized and coexpressed in *E. coli* with ZmAN2 and ZmKSL4 as well as the maize cytochrome P450 reductase ZmCPR2. Coexpression of the two diTPSs and ZmCPR2 without ZmCYP71Z16 served as a negative control. When all four enzymes were coexpressed, the presence of ZmCYP71Z16 resulted in the conversion of dolabradiene into two new products with fragmentation patterns featuring m/z 288 (compound **13**) and m/z 304 (compound **14**) mass ions that are characteristic of diterpenoid scaffolds containing one and two oxygen atoms, respectively (Fig. 3). High-resolution liquid chromatography-mass spectrometry (LC-MS) analysis identified the exact mass of compound **14** as m/z 304.2478, consistent with the molecular formula $C_{20}H_{32}O_2$. Subsequent HPLC

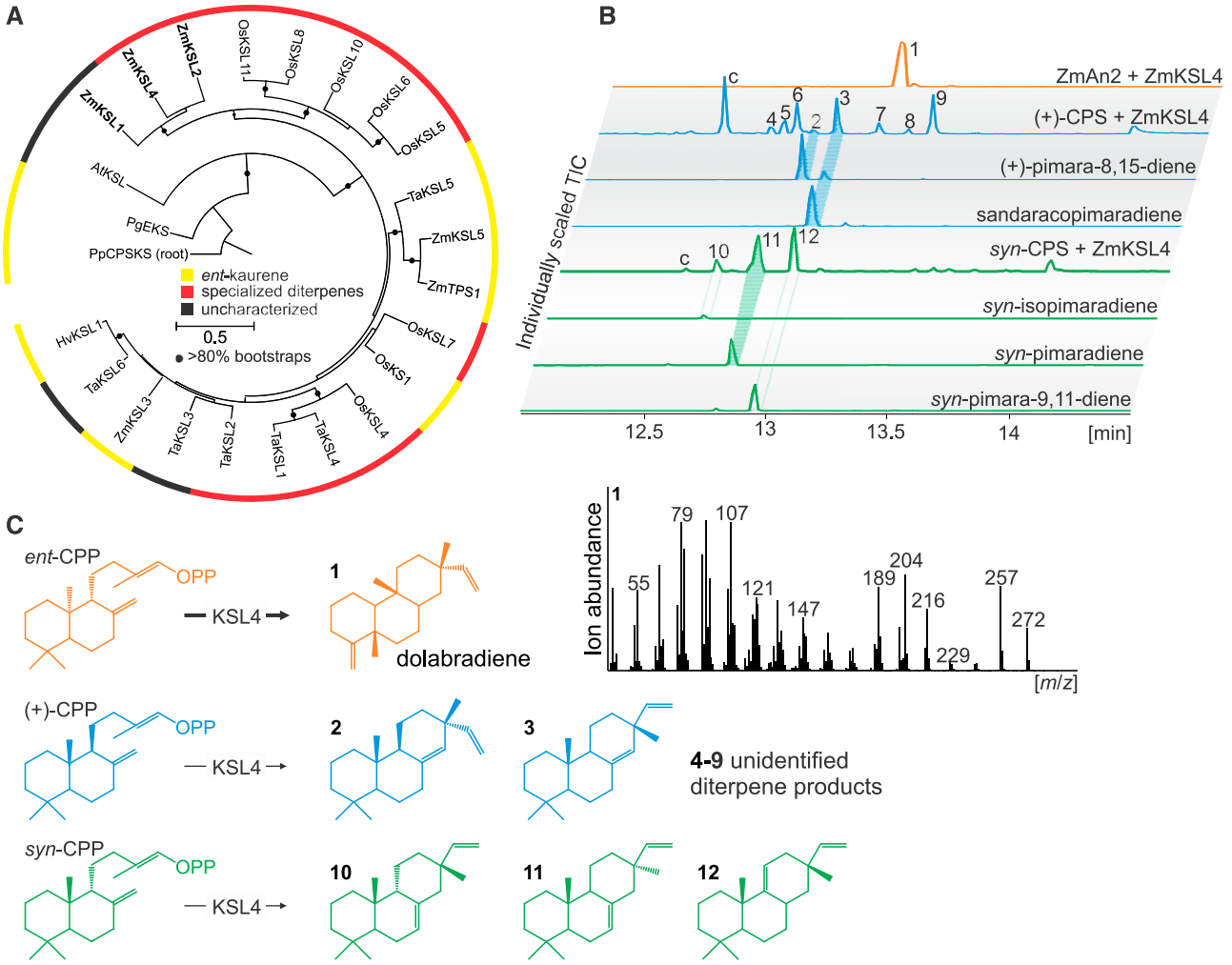

Figure 2. Functional characterization of the maize diterpene synthase ZmKSL4. A, Maximum likelihood phylogenetic tree of select monocot class I diTPSs (Supplemental Table S2). The tree is rooted with the ancestral *Physcomitrella patens ent*-kaurene synthase. Circles indicate bootstrap support of greater than 80% (500 repetitions), and the functional association with the biosynthesis of *ent*-kaurene (yellow) or specialized diterpenoids (red) is highlighted. B, Total ion chromatograms (TIC) of reaction products resulting from *E. coli* coexpression assays of ZmKSL4 with ZmAN2 CPP synthase (Harris et al., 2005), rice CPS4 *syn*-CPP synthase (Xu et al., 2004), and the grand fir abietadiene synthase variant D621A producing (+)-CPP (Peters and Croteau, 2002) as compared with available authentic standards for product identification. Compound **c** represents a contamination product from the engineered *E. coli* system. C, Major products of ZmKSL4 from prenyl diphosphate intermediates of *ent*-, normal (+)-, and *syn*-stereochemistry. The mass spectrum of dolabradiene **1** resulting from the coupled activity of ZmAN2 and ZmKSL4 is shown, and the structure of dolabradiene is depicted as verified by NMR analysis.

purification of compounds **13** and **14** followed by NMR analysis verified the structures as 15,16-epoxydolabrene (epoxydolabrene) and epoxydolabranol, respectively (Fig. 3; Supplemental Fig. S4). The biochemical characterization of ZmCYP71Z16 adds a previously unknown function to the diverse activities of members of the plant CYP71 family, facilitating the regiospecific oxygenation of dolabradiene at C-3 and C-16, presumably in a sequential reaction process. The formation of the monoepoxide **13,** in the absence of detectable formation of a monohydroxyl intermediate, is consistent with a P450 reaction sequence of epoxidation at C-16 prior to hydroxylation at C-3. To further investigate the catalytic activity of ZmCYP71Z16, we performed *E. coli* coexpression assays with ZmCPR2 and fed 10 μM purified epoxydolabrene and epoxydolabranol to the culture 5 h post induction. Expectedly, no new products were identified when feeding epoxydolabranol to the culture. In contrast, epoxydolabrene was converted to the hydroxylated derivative (Supplemental Fig. S5), supporting our proposed reaction sequence from epoxydolabrene to epoxydolabranol.

The phylogenetic relatedness of ZmCYP71Z16 and the previously reported zealexin-forming ZmCYP71Z18 (Mao et al., 2016) indicated that ZmCYP71Z16 may

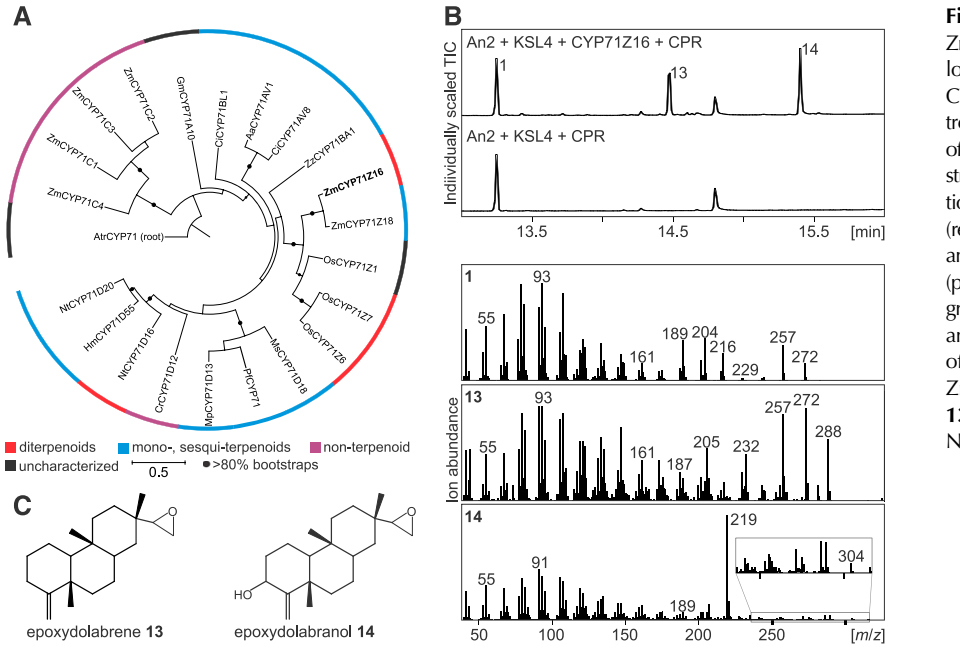

Figure 3. Functional characterization of ZmCYP71Z16. A, Maximum likelihood phylogenetic tree of select P450 proteins of the CYP71 family (Supplemental Table S2). The tree is rooted with an uncharacterized CYP71 of *Amborella trichopoda*. Circles indicate bootstrap support of greater than 80% (500 repetitions). Demonstrated activities in diterpenoid (red), monoterpenoid/sesquiterpenoid (blue), and other specialized metabolic pathways (purple) are highlighted. B, Total ion chromatograms (TIC) and mass spectra of products **1**, **13**, and **14** derived from microbial coexpression of ZmAN2, ZmKSL4, ZmCYP71Z16, and ZmCPR2. C, Structures of epoxydolabrene **13** and epoxydolabranol **14** as verified by NMR analysis.

be active on other substrates beyond a role in epoxydolabranol biosynthesis. To test this hypothesis, we conducted *E. coli* coexpression assays of ZmCYP71Z16 with ZmCPR2 and ZmTPS11, which form the zealexin precursor β-macrocarpene (Köllner et al., 2008b; Huffaker et al., 2011). This enzyme combination resulted in the formation of zealexin A1 (Supplemental Fig. S6). Reciprocal *E. coli* coexpression assays of ZmCYP71Z18 with ZmAN2 and ZmKSL4 did not result in the detectable formation of epoxydolabrene, epoxydolabranol, or other diterpenoid products. Therefore, we tested the activity of ZmCYP71Z18 using yeast in vivo feeding assays in the strain BY4741 expressing ZmCPR2 and ZmCYP71Z18. After feeding 25 μM purified dolabradiene to the culture, partial conversion into epoxydolabranol was observed (Supplemental Fig. S6).

ZmAN2 Is Required for Dolabralexin Biosynthesis in Vivo

The above in vitro coexpression assays demonstrated that ZmAN2 and ZmKSL4 can function together as a duo of class II and class I diTPSs to afford the dolabradiene scaffold and its downstream derivatives (Fig. 2). To validate if ZmAN2 provides the *ent*-CPP intermediate converted by ZmKSL4 into dolabradiene in vivo, we measured the abundance of dolabradiene and epoxydolabranol in the *Zman2* mutant, which is deficient in kauralexins (Vaughan et al., 2015), and compared the metabolite levels with those in wild-type plants of the near-isogenic W22 inbred line. Consistent with a function of ZmAN2 in the formation of dolabralexins, no epoxydolabranol or dolabradiene was detectable in the *Zman2* mutant line, while dolabralexins were abundant in root tissue of wild-type plants (Supplemental Fig. S7). Thus, both kauralexins and dolabralexins require ZmAN2 activity in vivo.

Dolabralexins Are Abundant in Maize Root Tissue

To investigate if dolabralexins, derived from the coupled activity of ZmAN2, ZmKSL4, and ZmCYP71Z16, occur as abundant metabolites in planta, terpenoid metabolite profiling was performed on different maize varieties, including the inbred lines B73 and Mo17 and a commercial hybrid sweet corn (Golden Queen). LC-MS analysis of field-grown 70-d-old plants showed that both dolabradiene and epoxydolabranol were abundant in the roots of all tested genotypes (Fig. 4). Concentrations of both compounds differed between genotypes; however, epoxydolabranol was consistently more abundant than dolabradiene and displayed greater abundance in Mo17 (700 ± 68 ng g^{-1} fresh weight) and Golden Queen (507 ± 52 ng g^{-1} fresh weight) compared with B73 (62 ± 7 ng g^{-1} fresh weight).

Alongside epoxydolabranol, we observed an additional earlier eluting and predictably more polar metabolite at high abundance in maize roots, with concentrations of 60 ± 18.5 μg g^{-1} fresh weight in Mo17, 212 ± 34 μg g^{-1} fresh weight in Golden Queen, and 41 ± 4 μg g^{-1} fresh weight in B73 (Fig. 4; Supplemental Figs. S8 and S9). High-resolution LC-tandem mass spectrometry (MS/MS) analysis of this metabolite defined an accurate parent mass $[2M+H]^+$ of m/z 645.5. In addition, LC-MS and LC-MS/MS analyses revealed two notable features. First, the presence of substantial in-source decay led to a charged molecule of $[M\text{-}H_2O+H]^+$ m/z 305.25 and $[M\text{-}2H_2O+H]^+$ m/z 287.09 with an MS/MS fragmentation pattern similar to epoxydolabranol (Fig. 4). Second, MS/MS of the $[2M+H]^+$ m/z 645.5 parent ion

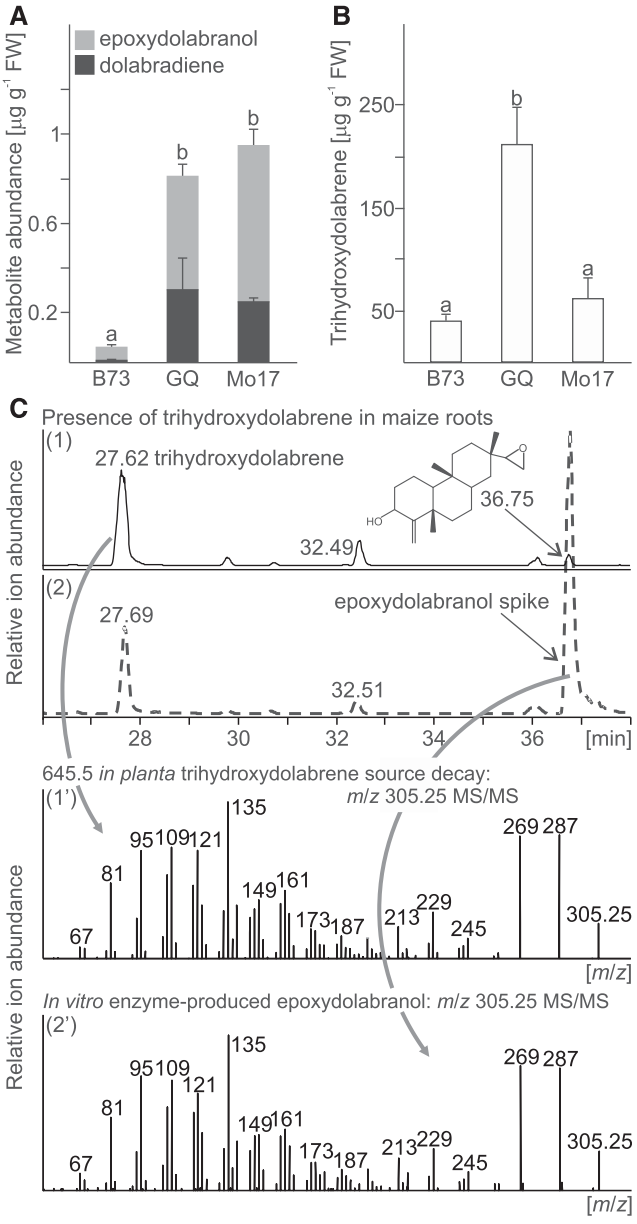

Figure 4. Occurrence of dolabralexins in planta. A and B, Average quantities of dolabradiene and epoxydolabranol (A) and trihydroxydolabrene (B) in field-grown roots of B73, Mo17, and hybrid sweet corn (Golden Queen [GQ]). Error bars represent propagated SE values across four biological replicates. Letters represent significant differences at $P < 0.05$ as measured using ANOVA and Tukey's tests to correct for multiple comparisons between control and treatments. FW, Fresh weight. C, Analysis of trihydroxydolabrene extracted from roots using LC-MS/MS analysis, with traces representing combined extracted ion chromatograms (m/z 305–305.5 + 645.25–645.75). In-source decay of the $[2M+H]^+$ m/z 645.5 trihydroxydolabrene parent ion yields $[M-H_2O+H]^+$ m/z 305.25, occurring at a retention time of 27.6 min. MS/MS analyses of the trihydroxydolabrene-derived m/z 305.25 results in highly similar fragmentation patterns as compared with the enzyme-produced epoxydolabranol analytical standard (retention time = 36.7 min).

yielded closely related spectra m/z 305.25 and 287.09, as seen for epoxydolabranol (Supplemental Fig. S8). Under markedly different LC-MS conditions, an alternative predominant candidate parent ion $[M+Na+H]^+$ m/z 345 was obtained (Supplemental Fig. S9). To elucidate the precise identity of the dolabradiene-related metabolite, a large-scale methanol (MeOH) extraction of mature field-grown maize roots was subjected sequentially to C18 flash chromatography and semi-preparative HPLC with LC-MS-based monitoring of factions using the $[M+Na+H]^+$ m/z 345 candidate parent ion (Supplemental Fig. S9). A purified 300-μg sample dissolved in deuterated dimethyl sulfoxide (d_6-DMSO) was used for ^{1}H-NMR, and carbon chemical shift assignments were based on heteronuclear single quantum correlation (HSQC) and heteronuclear multiple bond correlation (HMBC) analyses (Supplemental Fig. S10). Collectively, all data are consistent with trihydroxydolabrene ($C_{20}H_{34}O_3$; exact mass, m/z 322.25) representing a hydrolysis of the epoxy group of epoxydolabranol, which accumulates as the dominant dolabralexin pathway metabolite. Predictably, trihydroxydolabrene was present at only trace levels in *Zman2* mutant plants as compared with control plants (Supplemental Fig. S7).

Dolabralexins Are Induced in Biotic and Abiotic Stress Responses

Following the detection of dolabradiene, epoxydolabranol, and trihydroxydolabrene in planta, we quantified the accumulation of all three compounds in roots of 16-d-old Golden Queen seedlings under abiotic stress conditions. Root treatments with 1 mM $CuSO_4$ were used as a proxy for oxidative stress compared with controls treated with water only. The accumulation of dolabradiene and epoxydolabranol was detected between 4 and 48 h post $CuSO_4$ treatment and increased to a concentration of ~160 ng g^{-1} fresh weight epoxydolabranol at 48 h (Fig. 5). Notably, trihydroxydolabrene was detected as the dominant metabolite in $CuSO_4$-challenged roots, reaching concentrations greater than 100 μg g^{-1} fresh weight. Consistent with inducible dolabralexin accumulation, gene expression analysis via quantitative real-time PCR of *ZmAN2*, *ZmKSL4*, and *ZmCYP71Z16* revealed increased transcript levels of all three genes from 2 to 12 h, with *ZmAN2* showing the most significant up-regulation of ~400-fold (Fig. 5).

We next investigated the accumulation of dolabralexins in the response of maize to elicitation with *Fusarium verticillioides* and *Fusarium graminearum*, which are causal agents of seedling blights, stalk rots, ear rots, and mycotoxin contamination (Munkvold, 1997; Goswami and Kistler, 2004; Baldwin et al., 2014). For this purpose, roots of 53-d-old Mo17 plants were inoculated with live *F. verticillioides* or *F. graminearum* spores and harvested for the analysis of both metabolites and transcripts 7 d later. Controls were performed with roots wounded and treated with water alone. Upon

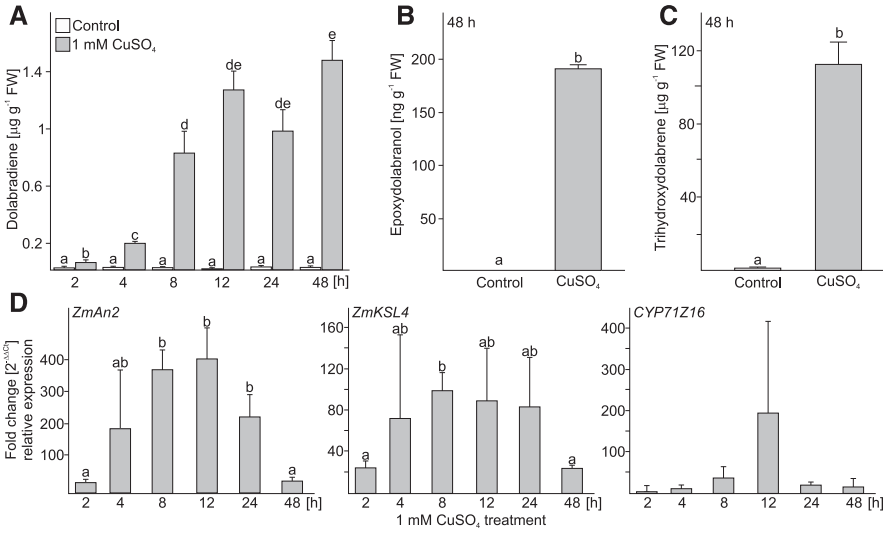

Figure 5. Accumulation of dolabralexins in response to abiotic stress. A to C, Average quantities of dolabradiene (A), epoxydolabranol (B), and trihydroxydolabrene (C) in maize (Golden Queen) roots treated with either water (Control) or 1 mM $CuSO_4$ over a period of 48 h. FW, Fresh weight. D, Fold change ($2^{-\Delta\Delta Ct}$) of the transcript abundance of *ZmAN2, ZmKSL4,* and *ZmCYP71Z16* in the same root tissues used for diterpenoid analyses. Gene expression was measured by quantitative real-time PCR and normalized to the internal reference *EF1-α*. Primer efficiency was verified by dissociation curves and sequence verification of representative products. Letters (a–e) represent significant differences at $P < 0.05$ as measured using ANOVA and Tukey's tests to correct for multiple comparisons between control and treatments. Error bars represent propagated SE values ($n = 4$).

inoculation with *F. verticillioides* or *F. graminearum* spores, dolabradiene accumulation was induced 6- or 45-fold, respectively, compared with wounded plants (Fig. 6). Similarly, epoxydolabranol accumulation was increased 55- and 79-fold, respectively, in response to the two *Fusarium* species. Moreover, in response to *F. verticillioides* and *F. graminearum*, trihydroxydolabrene accumulated 14- and 32-fold greater compared with control plants treated by wounding only. Trihydroxydolabrene reached concentrations of up to 225 $\mu g\ g^{-1}$ fresh weight in elicited root tissue. By comparison, kauralexin A- and B-series metabolites accumulated to approximately 9 $\mu g\ g^{-1}$ fresh weight in response to pathogen infection in the same mature root tissues. Consistent with the pathogen-inducible accumulation of dolabralexins, the transcript abundance of *ZmAN2* and *ZmKSL4* increased upon fungal elicitation while *ZmCYP71Z16* showed no up-regulated gene expression at this 7-d time point (Fig. 6).

Dolabralexins Are Active against Fungal Pathogens

To further assess the predicted defense-related roles for dolabralexins, in vitro antimicrobial assays were performed with *F. verticillioides* and *F. graminearum*. The growth of fungal hyphae in the presence and absence of purified epoxydolabranol and trihydroxydolabrene was measured in defined liquid medium using an established 96-well microtiter assay (Schmelz et al., 2011). Based on previous maize diterpenoid bioassays and the quantified in vivo abundance of epoxydolabranol and trihydroxydolabrene (Figs. 4–6), we utilized 10 and 50 $\mu g\ mL^{-1}$ as relevant local tissue concentrations to test for antimicrobial activity. After 48 h, epoxydolabranol at 10 and 50 $\mu g\ mL^{-1}$ substantially reduced the growth of *F. graminearum* by 41% and 87%, respectively, and likewise inhibited the growth of *F. verticillioides* by 24% and 71%, respectively (Fig. 7). We further assessed the antimicrobial efficacy of trihydroxydolabrene at concentrations of 10 to 100 $\mu g\ mL^{-1}$, well below those detectable in planta. In contrast to epoxydolabranol, trihydroxydolabrene had no inhibitory activity on the growth of *F. graminearum* but resulted in a dose-dependent growth reduction of *F. verticillioides* at concentrations of 10 $\mu g\ mL^{-1}$ (9%), 50 $\mu g\ mL^{-1}$ (15%), and 100 $\mu g\ mL^{-1}$ (21%).

DISCUSSION

The combination of extreme and shifting biotic and abiotic stresses can overwhelm the natural defense systems of plants and result in substantial yield losses in staple crops (Chakraborty and Newton, 2011; de Sassi and Tylianakis, 2012). An improved understanding of the inherent strengths and weaknesses that underlie mechanisms of crop resilience can mitigate yield loss. For example, detailed knowledge of terpenoid metabolism, the underlying genes, and their contribution to maize stress resilience could provide useful resources for improving crop traits (Degenhardt et al., 2009). This study highlights the utility of integrating genomics and metabolomics with both in vivo and in vitro biochemical approaches to elucidate defense pathways in well-studied crop plants. We identified

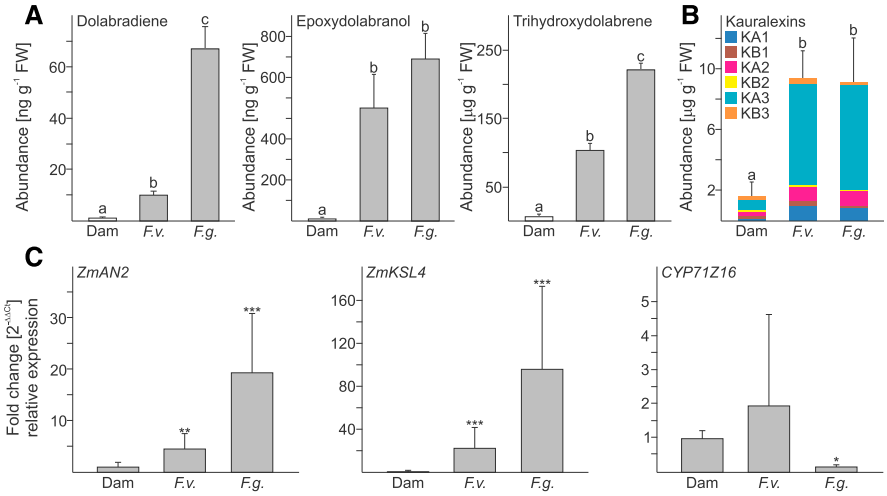

Figure 6. Accumulation of dolabralexins in response to biotic stress. A, Average (n = 4) quantities of dolabradiene, epoxydolabranol, and trihydroxydolabrene in Mo17 roots damaged (Dam) and treated with water or inoculated separately with *F. verticillioides* (*F.v.*) or *F. graminearum* (*F.g.*). Treatments occurred in 53-d-old plants with tissue harvests 7 d later. B, Quantification of A-series (KA) and B-series (KB) kauralexin metabolites in the same tissue samples. Error bars represent propagated SE values. Letters represent significant differences at $P < 0.05$ as measured using ANOVA and Tukey's tests to correct for multiple comparisons between control and treatments. FW, Fresh weight. C, Fold change ($2^{-\Delta\Delta Ct}$) of the transcript abundance of *ZmAN2*, *ZmKSL4*, and *ZmCYP71Z16* in the corresponding Mo17 roots normalized to the internal reference gene *EF1-α*. Error bars represent propagated SE values of the biological replicates. Asterisks indicate significant changes compared with wounded tissue at $P < 0.0005$ (***), $P < 0.01$ (**), and $P < 0.1$(*).

functions for the combined pathway of the maize diTPSs ZmAN2 and ZmKSL4 and the cytochrome P450 ZmCYP71Z16 that fuel diterpenoid metabolism and the production of dolabralexins. Dolabralexins and corresponding pathway genes are strongly stress inducible, consistent with roles in protecting and buffering against the negative impacts of biotic and abiotic stresses.

The dolabralexin precursor, dolabradiene, was reported previously in only a few coniferous trees of the Araucariaceae and Cupressaceae families (Brophy et al., 2000; Takahashi et al., 2001), and its biological role in these species is unknown. Thus, based on current knowledge and the absence of dolabralexin in other major Poaceae crops, such as rice and wheat, the inferred emergence of the dolabralexin biosynthetic pathway occurred after the evolutionary separation of maize from wheat and rice approximately 50 million years ago (Wolfe et al., 1989; Grass Phylogeny Working Group II, 2012).

Mechanistically, we propose a pathway for the biosynthesis of epoxydolabranol that proceeds through ZmKSL4-catalyzed ionization-dependent cyclization of *ent*-CPP via an *ent*-dolabra-15-en-4-yl$^+$ carbocation to afford dolabradiene and subsequent P450-catalyzed functional modification of the latter (Fig. 8). Dolabradiene production via microbial coexpression of ZmAN2 and ZmKSL4 combined with the absence of dolabralexins in the established *Zman2* mutant substantiates our hypothesis that ZmAN2 provides the *ent*-CPP substrate for dolabradiene formation. This also is consistent with previous work demonstrating a role of ZmAN2 in specialized metabolism (Harris et al., 2005).

From *ent*-CPP, the reaction will inevitably proceed via the common pimaren-8-yl$^+$ carbocation, as shown for other labdane-related diterpene scaffolds (Peters, 2010). Dolabradiene formation then can be achieved through sequential C-9,8-hydride shift, methyl migration from C-10 to C-9, C-5,10-hydride shift, and another methyl transfer from C-18 to C-5 to yield the *ent*-dolabra-15-en-4-yl$^+$ intermediate (Peters, 2010), deprotonation of which gives rise to dolabradiene (Fig. 8). By contrast, the formation of *ent*-kaurene and *ent*-iso-kaurene, as precursors of GAs and kauralexins, respectively, would proceed through secondary cyclization of the pimaren-8-yl$^+$ carbocation followed by ring rearrangement to afford the tetracyclic kauranyl scaffold (Xu et al., 2007b). Subsequent to *ent*-dolabra-15-en-4-yl$^+$ formation, ZmCYP71Z16-enabled sequential epoxidation at C-16 and hydroxylation at C-3 yields epoxydolabranol. The detection of epoxydolabrene and epoxydolabranol, but not a 3β-hydroxydolabrene intermediate, combined with the ZmCYP71Z16-catalyzed conversion of epoxydolabrene to epoxydolabranol in in vitro feeding assays, supports a reaction sequence where the epoxide group is formed prior to hydroxylation. Epoxydolabranol is further converted into trihydroxydolabrene via either enzymatic or spontaneous hydrolysis. The presence of trihydroxydolabrene at high concentrations suggests that the characterized products of ZmAN2/ZmKSL4/ZmCYP71Z16 do not represent dominant pathway end products but, instead, may serve as intermediates to trihydroxydolabrene and possibly more complex and increasingly polar maize diterpenoids.

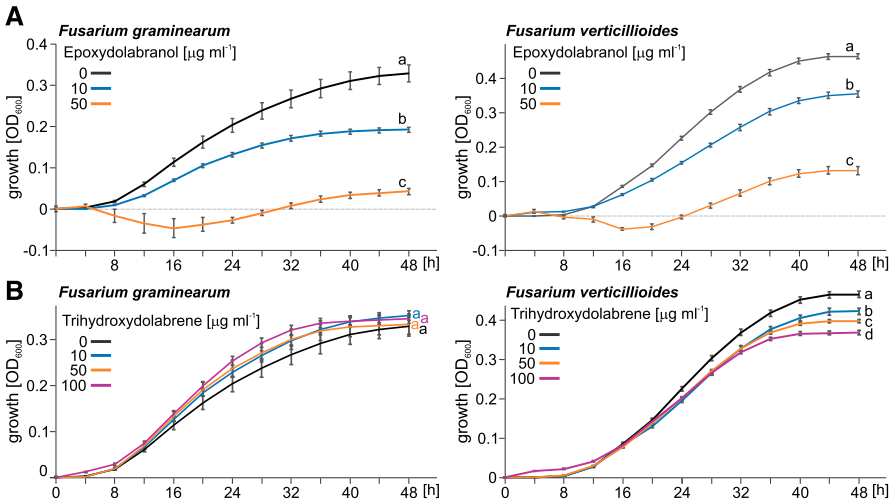

Figure 7. Antifungal activity of dolabralexins. Average growth (OD_{600}) of *F. graminearum* and *F. verticillioides* is shown in the absence and presence of purified epoxydolabranol (A) and trihydroxydolabrene (B) measured over a 48-h time course in defined minimal broth medium using a microtiter plate assay. Error bars represent propagated SE values ($n = 6$), and letters (a–d) represent significant differences at $P < 0.05$ as measured using ANOVA and Tukey's tests to correct for multiple comparisons between control and treatments.

Previous studies demonstrated that *Zman2* lacks pathogen-elicited diterpenoids of the kauralexin class (Vaughan et al., 2015). Our results demonstrate that this mutant also is deficient in dolabralexin biosynthesis (Supplemental Fig. S7) and suggest a biosynthetic interconnectivity and potential biosynthetic competition between the kauralexin and dolabralexin pathways. *ZmAN2* was first described in a differential display analysis of highly elicited transcripts following *F. graminearum* challenge of maize silks (Harris et al., 2005). Following the first description of ZmAN2, pathogen-elicited transcripts have been observed and reported in a large number of maize studies with diverse microbes (Huffaker et al., 2011; Schmelz et al., 2011, 2014; van der Linde et al., 2011; Vaughan et al., 2014; Christie et al., 2017). The nearly ubiquitous presence of *ZmAN2* as a pathogen defense transcript marker is consistent with the essential biosynthetic role in the modular formation of multiple specialized diterpenoid metabolites, including not only A- and B-series kauralexins (Schmelz et al., 2011) but also dolabralexins. Notably, *ZmAN2* does not cluster with any class I diTPSs in the maize genome, illustrating a different genomic organization of diterpenoid metabolism in maize as compared with rice and tomato (*Solanum lycopersicum*), where several specialized diterpenoid pathways form functional biosynthetic clusters (Matsuba et al., 2013; Nützmann et al., 2016). However, the presence of the uncharacterized class II diTPSs ZmCPS3 and ZmCPS4 suggests that specialized diterpenoid metabolism in maize likely follows the common modular blueprint of combining different diTPS and P450 enzymes, as shown for rice, wheat, and various other species across the plant kingdom (Xu et al., 2007a; Zhou et al., 2012; Hall et al., 2013; Cui et al., 2015; Zerbe and Bohlmann, 2015). This hypothesis is substantiated by (1) the in vitro substrate promiscuity of ZmKSL4 with CPP of *ent-*, *syn-*, and (+)-stereochemistry and (2)

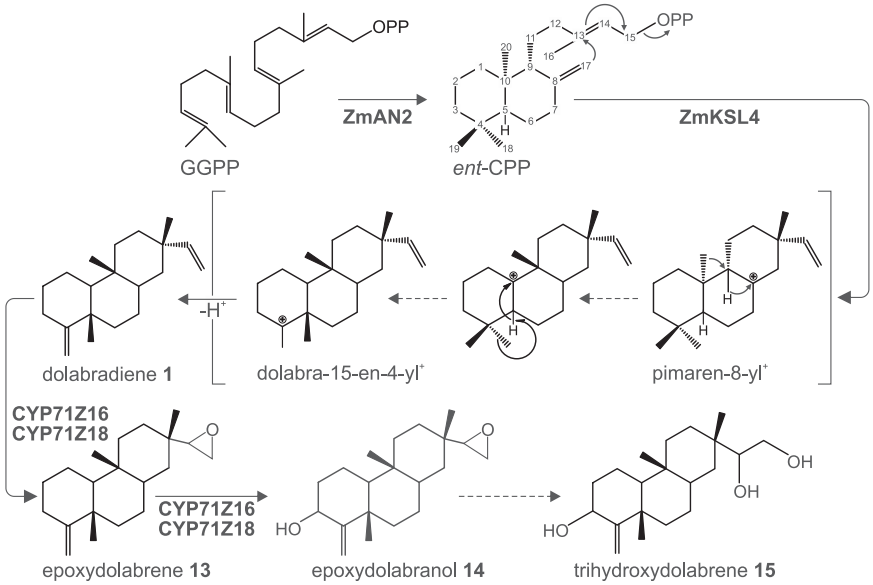

Figure 8. Biosynthesis of maize dolabralexins. Shown is a proposed biosynthetic pathway of dolabralexins through the sequential activity of ZmAN2, ZmKSL4, and ZmCYP71Z16.

the capacity of ZmCYP71Z16 and ZmCYP71Z18 (previously reported to function in zealexin biosynthesis; Mao et al., 2016) to convert both sesquiterpenoid and diterpenoid intermediates (Supplemental Fig. S6). Consistent with their largely redundant substrate promiscuity, the *ZmCYP71Z16* and *ZmCYP71Z18* genes are located directly adjacent to each other on chromosome 5, suggesting that these P450s emerged from a more recent gene duplication event observed frequently in specialized diterpenoid metabolism (Zi et al., 2014) and may have overlapping or complementary functions in vivo.

The occurrence of dolabralexins in field-grown maize roots and their accumulation in response to abiotic and biotic stresses encourage a more extensive exploration of biological roles in planta. In the context of biotic stress, epoxydolabranol (albeit at moderately higher concentrations than observed in planta) inhibits the growth of two major maize *Fusarium* spp. pathogens with a comparable potency, as demonstrated earlier for the kauralexins (Schmelz et al., 2011). These findings are supported by a recent study demonstrating increased disease susceptibility to *F. verticillioides* in *Zman2* mutants. However, due to the critical role of ZmAN2 in kauralexin and dolabralexin biosynthesis, this result does not address the specific roles of kauralexin and dolabralexin pathway branches (Christensen et al., 2018). The apparent yet lower antimicrobial potency of trihydroxydolabrene at concentrations below those observed in elicited plant tissues, and the specificity of trihydroxydolabrene activity to *F. verticillioides*, highlight the importance of the C-15,16 epoxy group for bioactivity. These results suggest distinct protective functions and biological roles for individual dolabralexins. The inducible accumulation of dolabralexins in response to oxidative and pathogen stress is consistent with dual functionality in abiotic and biotic stress responses, similar to the kauralexin and zealexin pathways (Huffaker et al., 2011; Schmelz et al., 2011; Vaughan et al., 2015). Recent findings enabled by mutant analyses highlight an important yet thus far rarely proven role of diterpenoids in protecting roots against environmental perturbations. For example, *Zman2* mutant plants were more susceptible to drought stress than the corresponding wild-type plants (Vaughan et al., 2015). While this impact was attributed to kauralexin deficiency, the discovery of the dolabralexins now forces the consideration of multiple ZmAN2-dependent pathway branches to understand responses to drought and belowground stresses. This hypothesis is supported further by the quantification of predominant dolabralexins accumulating in challenged roots. For example, in pathogen-challenged roots, trihydroxydolabrene is present at 20-fold greater levels than established kauralexins. In contrast, the induced accumulation of kauralexins was shown previously in stems and scutella tissues to exceed 100 μg g^{-1} fresh weight as compared with the 10 μg g^{-1} fresh weight currently detected in mature roots (Schmelz et al., 2011). Notably, *ZmAN2* is located proximal to a quantitative trait locus mapped to bin 1.03 that is associated with root growth (Rahman et al., 2011), and *ZmKSL4* colocates in bin 1.08 with quantitative trait loci associated with both drought tolerance (Tuberosa et al., 2002) and abscisic acid biosynthesis, which can further mediate drought-induced phytoalexin biosynthesis in maize roots (Vaughan et al., 2015). Our findings here contribute to a growing body of knowledge demonstrating roles for root diterpenoids, including momilactone phytoalexins in rice (Toyomasu et al., 2008), the antiherbivory activity of rhizathalene in Arabidopsis (*Arabidopsis thaliana*; Vaughan et al., 2013), and drought tolerance mediated by isorosmanol in rosemary (*Rosmarinus officinalis*; Munné-Bosch and Alegre, 2000).

The existence of an abundant novel maize root defense, as well as significant and distinct antifungal activities for epoxydolabranol and trihydroxydolabrene in vitro, merit a closer examination of the precise ecological functions of dolabralexins. Such studies will ultimately require multiple genetic mutants of *ZmKSL4* and *ZmCYP71Z16/18* in future work. While historically recalcitrant to discovery, the complex modular networks of diterpenoid defense pathways in maize, rice, and possibly other cereal crops are import to understanding ecological interactions and the genetic basis of crop stress resilience (Schmelz et al., 2014).

MATERIALS AND METHODS

Plant and Fungal Materials

Seeds of hybrid maize (*Zea mays* variety Golden Queen; Southern States Cooperative), landrace inbreds (B73, Mo17, and W22; National Genetic Resources Program, Germplasm Resources Information Network), and a *Ds* insertion mutant, *Zman2* (Vaughan et al., 2015), were germinated in MetroMix 200 (Sun Gro Horticulture) supplemented with 14-14-14 Osmocote (Scotts Miracle-Gro) and grown as described previously (Schmelz et al., 2009). Field-challenged roots from B73, Mo17, Ky21, and hybrid sweet corn grown at the Biology Field Station at the University of California, San Diego, during the summer of 2016 were recovered 75 d after planting, washed, frozen in liquid N_2, ground to a fine powder, and ultimately used for metabolite analysis. Fungal stock cultures of *Fusarium verticillioides* (Northern Regional Research Laboratory; NRRL stock no. 7415) and *Fusarium graminearum* (NRRL stock no. 31084) were grown on V8 agar for 2 to 3 weeks before the quantification and use of spores (Huffaker et al., 2011).

Isolation and Cloning of cDNAs

Total RNA was extracted from ground tissue of young maize (B73) seedlings as described previously (Chourey et al., 2010). For cloning of *ZmKSL4*, *ZmCYP71Z18*, and *ZmTPS11*, 5 μg of total RNA was reverse transcribed using qScript cDNA SuperMix (Quanta Biosciences) followed by PCR amplification of the target genes with gene-specific oligonucleotides (Supplemental Table S1). The amplified full-length genes of *ZmTPS11* and *ZmCYP71Z18* and an N-terminally truncated form of *ZmKSL4* (*ZmKSL4Δ106*, lacking the predicted plastidial transit peptide) were ligated with the zero Blunt II-TOPO vector (Invitrogen) and transformed into TOP 10 chemically competent cells for plasmid isolation and sequence verification. *ZmKSL4* was subcloned further into the expression vectors pET28b(+) and pCOLA-DUET (Novagen/EMD) for coexpression in *Escherichia coli*. *ZmTPS11* was inserted into the vector pCOLA-DUET for expression in *E. coli*. *ZmCYP71Z18* was subcloned into pET28b(+) and pCOLA-DUET, as well as pESC-Leu-2D (Stratagene), for expression in *E. coli* and *Saccharomyces cerevisiae*, respectively. In addition, codon-optimized genes for the full-length sequences of maize *FARNESYL DIPHOSPHATE SYNTHASE3* (*ZmFPPS3*) and *ZmCPR2*, as well as a modified version of *ZmCYP71Z16* (32 N-terminal residues replaced with

the leader sequence MAKKTSSKGK), were obtained from the Department of Energy Joint Genome Institute through Community Science Program grant WIP2568 (Supplemental Table S1). *ZmCYP71Z16* and *ZmCPR2* were inserted into the multiple cloning sites of the pET-DUET1 vector (Novagen/EMD) to generate the plasmid pET-DUET1:ZmCPR2/ZmCYP71Z16 for expression in *E. coli*. *ZmFPPS3* was subcloned into the vector pCOLA-DUET together with *ZmTPS11* for expression in *E. coli*.

Quantitative Real-Time PCR

Gene expression analyses of *ZmAN2*, *ZmKSL4*, and *ZmCYP71Z16* were performed using the same $CuSO_4$-treated or *Fusarium* spp.-inoculated roots as described for terpenoid profiling. Total RNA was isolated as described previously (Kolosova et al., 2004). First-strand cDNA was synthesized using the SuperScript III First-Strand Synthesis Kit (Invitrogen) and oligo(dT) primers according to the manufacturer's instructions. Transcript levels were quantified with a Bio-Rad C1000 Touch Thermo Cycler interfaced with a CFX96 Real-Time System and iTaq Universal SYBR Green Supermix (Bio-Rad) according to the manufacturer's protocols with 5 ng μL^{-1} cDNA and 300 nM oligonucleotides. Mean cycle threshold values of two technical and three biological replicates were normalized using elongation factor *EF1-α* as a reference gene. Fold change values were calculated using the $2^{-\Delta\Delta Ct}$ method. Gene-specific oligonucleotides are listed in Supplemental Table S1.

Combinatorial Expression in *E. coli*

The functional coexpression of enzymes was carried out using a previously described *E. coli* system engineered for enhanced diterpenoid production (Morrone et al., 2010; Kitaoka et al., 2015). For biochemical characterization of ZmKSL4, the N-terminally truncated gene in the expression vector pET28b(+) or pCOLA-DUET was cotransformed in *E. coli* BL21DE3-C41 cells (Lucigen) with a plasmid carrying a geranylgeranyl diphosphate synthase and constructs of class II diTPSs with different products: ZmAN2 forming *ent*-CPP (pGGeC), rice (*Oryza sativa*) CPS4 producing *syn*-CPP (pGGsC), or a variant of grand fir (*Abies grandis*) abietadiene synthase forming (+)-CPP (pGGnC; Morrone et al., 2010). For additional coexpression of ZmCYP71Z16, the codon-optimized construct pET-DUET1:ZmCPR2/ZmCYP71Z16 was coexpressed with pGGeC and pET28b:ZmKSL4Δ106. For analysis of zealexin formation, the construct pET-DUET1:ZmCPR2/ZmCYP71Z16 was coexpressed with ZmFPPS3 and the *β*-macrocarpene synthase TPS6 (Köllner et al., 2008b; Richter et al., 2015) as well as the enhancer plasmid pIRS (Morrone et al., 2010). All coexpression assays were performed in *E. coli* BL21DE3-C41 and grown in 45 mL of Terrific Broth medium to an OD_{600} of ~0.6 at 37°C. Cultures were cooled to 16°C before induction with 1 mM isopropyl-thiogalactoside and incubation for 72 h with supplements of 1 mM $MgCl_2$ and 25 mM sodium pyruvate. For P450 coexpression, cultures were supplemented further with 4 mg L^{-1} riboflavin and 75 mg L^{-1} δ-aminolevulinic acid. Enzyme products were extracted with 50 mL of 100% hexane or 1:3 ethyl acetate:hexane, concentrated under an N_2 stream, and resuspended in 1 mL of hexane for gas chromatography (GC)-MS analysis.

Yeast Whole-Cell Activity Assays

To analyze the catalytic specificity of ZmCYP71Z18 (Mao et al., 2016), the full-length construct was coexpressed with ZmCPR2 in *S. cerevisiae* strain BY4741 (Jensen et al., 2011; Mao et al., 2016). Whole-cell assays were conducted as reported earlier (Pompon et al., 1996). In brief, cells were grown in 50 mL of selective dropout medium (−Leu, with 2% [w/v] dextrose) at 30°C to an OD_{600} of ~0.6, then transferred to selective dropout medium with 2% (w/v) Gal with further incubation for 5 h. Subsequently, cultures were supplemented with 25 μM dolabradiene or macrocarpene 1:1 MeOH:DMSO and incubated for 24 h prior to cell harvest and product extraction with diethyl ether (cell pellet) or ethyl acetate (supernatant). Extracts were dried, resuspended in 200 μL of MeOH, and derivatized with 10 μL of tetramethylsilane-diazomethane (Sigma-Aldrich) for 2 h. After drying under an N_2 stream and redissolving in hexane, samples were analyzed via GC-MS as described below.

GC-MS Analysis

GC-MS analysis of enzyme products was performed on an Agilent 7890B gas chromatograph with a 5977 Extractor XL MS Detector at 70 eV and 1.2 mL min^{-1} He flow, using an HP5-MS column (30 m, 250 μm i.d., 0.25 μm film) with a sample volume of 1 μL and the following GC parameters: pulsed splitless injection at 250°C and 50°C oven temperature; held at 50°C for 3 min, 20°C min^{-1} to 300°C, and held for 3 min. MS data from 90 to 600 *m/z* were collected after a 10-min solvent delay. For the analysis of dolabradiene present in plant samples, vapor phase extraction was used (Schmelz et al., 2004) for sample enrichment, and GC-MS analyses were conducted on an Agilent 6890 Series gas chromatograph coupled to an Agilent 5973 MS Detector. Separation was achieved on an Agilent DB-35MS column (30 m × 0.25 mm × 0.25 μm). Samples were introduced in splitless injection mode with an initial oven temperature of 45°C. The temperature was held for 2.25 min, then increased to 300°C with a gradient of 20°C min^{-1}, and held at 300°C for 5 min (interface temperature, 250°C; mass temperature, 150°C; source temperature, 230°C; electron energy, 70 eV). GC-(electron impact)-MS-based quantification of plant endogenous dolabradiene was based upon the slope of an external standard curve constructed from enzyme-produced and chemically purified dolabradiene using the diagnostic *m/z* 216 fragment ion. The identification of dolabradiene included the comparison of retention time (13.88 min) with the standard and the comparison of mass spectra with the Wiley, National Institute of Standards and Technology, and Adams libraries.

LC-MS Analysis of Dolabralexin Pathway Metabolites

Plant samples were ground to a fine powder with liquid N_2 and weighed out in 50-mg aliquots. LC-MS analyses of diterpenoids were performed as described elsewhere (Ding et al., 2017). In brief, tissue samples were sequentially and additively bead homogenized in (1) 100 μL of 1-propanol:acetonitrile (ACN):formic acid (1:1:0.01), (2) 250 μL of ACN:ethyl acetate (1:1), and (3) 100 μL of water. Aliquots were analyzed via LC-MS using an Agilent 1260 Infinity Series HiP Degasser (G4225A) with a 1260 binary pump (G1312B) and a 1260 autosampler (G1329B) with a binary gradient mobile phase consisting of 0.1% (v/v) formic acid in water and 0.1% (v/v) formic acid in MeOH on an Agilent Zorbax Eclipse Plus C_{18} Rapid Resolution HD column (1.8 μm, 2.1 × 50 mm; 0.35 mL min^{-1} flow rate). Eluted analytes underwent electrospray ionization via an Agilent Jet Stream Source with thermal gradient focusing using the following parameters: nozzle voltage (500 V), N_2 nebulizing gas (flow, 12 L min^{-1}; 55 p.s.i., 225°C), and sheath gas (350°C, 12 L min^{-1}). The transfer inlet capillary was 3,500 V, and both MS1 and MS2 heaters were at 100°C. Positive ionization $[M+H]^+$ mode scans (0.1-amu steps, 2.25 cycles s^{-1}) from *m/z* 100 to 1,000 were acquired. While the positive ion $[M+H]^+$ parent mass of epoxydolabranol was detectable with *m/z* 305, the predominant signal was consistent with a loss of water $[M\text{-}H_2O+H]^+$, namely *m/z* 287, with a stable retention time of 16.15 min. Absolute concentrations of compounds were calculated using external calibration curves of purified epoxydolabranol at concentrations ranging from 0.123 to 10 ng μL^{-1}. To estimate the quantities of trihydroxydolabrene, the predominant sodium adduct parent ion $[M+Na+H]^+$ *m/z* 345 was utilized, which additionally contained in-source decay fragment ions $[M\text{-}H_2O+H]^+$, $[M\text{-}2H_2O+H]^+$, and $[M\text{-}3H_2O+H]^+$ of *m/z* 305, 287, and 269, respectively. The complete ion series was functionally absent in all elicited *Zman2* samples, supporting parent-fragment interrelationships. Using the above instrument conditions, *m/z* 345 was used for quantification purposes in concert with an external standard curve of HPLC-purified trihydroxydolabrene.

For MS/MS analyses of trihydroxydolabrene, an Agilent 1100 HPLC device and locally made analytical column (using a custom pressure cell and 2.5-μm BEH C_{18} particle packed into fused silica capillary tubing with 200 μm i.d., 360 μm o.d., and 20 cm length) were integrated with a custom nanospray tip with an i.d. of less than 1 μm. Separation was achieved using a 60-min reverse-phase gradient: 0 to 1 min at 100% A (water and 0.1% formic acid), 1 to 26 min at 95% A and 5% B (ACN and 0.1% formic acid), 26 to 30 min at 5% A and 95% B (all w/v), and 31 to 60 min at 100% A. A splitter was used to split the flow rate from 0.2 to 0.6 mL min^{-1}. Spectra were acquired on a Q Exactive HF Orbitrap mass spectrometer (Thermo Electron), which was operated in positive ion mode with a spray voltage of 300 V, a source temperature of 275°C, and an S-lens radio frequency (RF) level set to 50%. A combined Top-N data-dependent scan and data-independent scan method was used to acquire high-resolution MS data. For data-dependent scans, each MS scan was followed by 10 MS/MS scans of the most intense ions from the parent MS scan. Mass resolutions of 60,000 and 15,000 were used for MS and MS/MS modes, respectively. An isolation window of 1 D and a normalized collision energy (NCE) of 30 were used for both data-dependent and data-independent scans.

NMR Analyses

For structural verification via NMR analysis, enzyme products were prepared as described above but using 500-mL cultures. Extracts were dried by

rotary evaporation and resuspended in suitable volumes of hexane prior to chromatographic purification by HPLC using an Agilent 1100 Series instrument with a diode array UV detector and an Agilent ZORBAX Eclipse Plus-C8 column (4.6 × 150 mm, 5 μm) at a 0.5 mL min^{-1} flow rate and a water/ACN gradient as mobile phase. Purified products were then dissolved in 0.5 mL of deuterated chloroform (Sigma-Aldrich), and NMR spectra were acquired at 25°C on a Bruker Avance III 800 spectrometer equipped with a 5-mm triple resonance cryo probe (CPTCI). Chemical shifts were calculated by reference to known deuterated chloroform (^{13}C 77.23 ppm, ^{1}H 7.24 ppm) signals offset from tetramethylsilane. All spectra were acquired using standard experiments on Bruker TopSpin 3.2 software, including 1D ^{1}H, 2D HSQC, correlation spectroscopy (COSY), and HMBC (600 MHz), and 1D ^{13}C spectra (201 MHz). For the purification of trihydroxydolabrene, 420 g of 75-d-old field-grown Ky21 root tissue was ground to a powder in liquid N_2, extracted with 500 mL of MeOH, filtered, and dried using a rotary evaporator. The resulting oily residue was then separated by preparative flash chromatography (CombiFlashRf; Teledyne ISCO) on a 15.5-g C18 (RediSepRf High Performance GOLD) column. The mobile phase consisted of solvent A (100% MilliQ water) and solvent B (100% ACN) with a continuous gradient of 0% to 100% B from 1 to 50 min using a flow rate of 19 mL min^{-1}. One-minute fractions were collected and analyzed by LC-MS. At 22 min (48% [v/v] ACN), a fraction highly enriched in trihydroxydolabrene was obtained. This fraction was purified further by HPLC using repeated 1-mg injections on a Zorbax RX-C18 (250 × 4.6 mm, 5 μm; Agilent) column and a mobile phase consisting of solvent A (ACN:water, 1:4) and solvent B (100% ACN) with a continuous gradient of A to B from 0 to 27 min using a flow rate of 1 mL min^{-1}. The recollected fractions spanning 15 to 16 min contained trihydroxydolabrene at approximately 85% purity and were used to generate samples for NMR, external standard curves for quantification, and antifungal bioassays. Purified trihydroxydolabrene was dissolved in d_6-DMSO (Cambridge Isotope Laboratories), and NMR spectra were acquired on a Bruker 600-MHz spectrometer equipped with a 1.7-mm CPTCI cryoprobe. Chemical shifts were calculated by reference to known d_6-DMSO (^{13}C 39.52 ppm, ^{1}H 2.50 ppm) signals. All spectra were acquired using standard experiments on a Bruker Avance III console and TopSpin 2.1.6 software, including 1D ^{1}H and 2D HSQC, COSY, and HMBC (600 MHz).

Abiotic Elicitation of Maize Roots with $CuSO_4$

Seeds of maize (Golden Queen) were germinated on wetted paper for 4 d at 23°C in the dark. Seedlings were then transferred to a hydroponic medium (Schmelz et al., 2001) and grown for 12 d under 16/8 h of light/darkness (28°C), light intensity of 180 μmol photons m^{-2} s^{-1}, and ~60% relative humidity. For the controlled exposure to oxidative stress, 1 mM $CuSO_4$ was added to the hydroponic medium. Root samples were collected at the indicated time points after treatment and frozen in liquid N_2 for metabolite and gene expression analyses.

Fungal Elicitation of Mature Maize Roots

For the root elicitation assays with live fungal pathogens (*Fusarium* spp.), large nodal roots (2 mm or greater diameter) of 53-d-old greenhouse plants, grown in separate 10-L pots and supplemented with 14-14-14 Osmocote (Scotts Miracle-Gro) fertilizer, were punctured with a blunt-ended circular steel pin (0.6 mm diameter) at 1-cm intervals and inoculated with 10 μL of either water or 1×10^7 conidia mL^{-1} *F. verticillioides* or *F. graminearum* at each wound site. In order to avoid mechanical damage to intentionally untreated tissues, treatments were limited to exposed roots growing along the outer edge of the soil in close contact with the vertical wall of the plastic pot. Seven days after inoculation, root samples were collected and frozen in liquid N_2 for metabolite and gene expression analysis.

In Vitro Antifungal Assays with Epoxydolabranol and Trihydroxydolabrene

Maize antifungal assays using epoxydolabranol and trihydroxydolabrene were performed using the Clinical and Laboratory Standards Institute M38-A2 guidelines as described previously (Schmelz et al., 2011). Briefly, fungal growth at 30°C in broth medium was monitored using a Synergy4 (BioTech Instruments) reader with a 96-well microtiter plate-based method through periodic measurements of changes in OD_{600}. Each well contained 200 μL of initial fungal inoculum (2.5×10^4 conidia mL^{-1}) with 0.5 μL of either pure DMSO or DMSO containing dilutions of HPLC-purified epoxydolabranol from in vitro assays and root-derived trihydroxydolabrene.

Phylogenetic Analysis

Protein sequence alignments (Supplemental Table S2) were performed using the CLCBio software package and curated with G-blocks (Talavera and Castresana, 2007). Maximum-likelihood phylogenetic trees were generated using PhyML version 3.0 (Guindon et al., 2010) with four rate substitution categories, LG substitution model, BIONJ starting tree, and 500 bootstrap repetitions.

Accession Numbers

Nucleotide sequences of characterized enzymes are available at the GenBank/EBI Data Bank with accession numbers DAA49845 (ZmKSL4), AFW68701 (ZmCYP71Z16), and AFW59698 (ZmCPR2) or the MaizeGDB server with accession numbers GRMZM2G061922 (ZmKSL4), GRMZM2G067591 (ZmCYP71Z16), and GRMZM2G104294 (ZmCPR2).

Supplemental Data

The following supplemental materials are available.

Supplemental Figure S1. Chromosomal locations of maize diTPS and P450 genes.

Supplemental Figure S2. NMR analysis of dolabradiene.

Supplemental Figure S3. Mass spectra of ZmKSL4 reaction products.

Supplemental Figure S4. NMR analysis of the ZmCYP71Z16 reaction products.

Supplemental Figure S5. Feeding assays of ZmCYP71Z16.

Supplemental Figure S6. Substrate specificity of ZmCYP71Z16 and ZmCYP71Z18.

Supplemental Figure S7. Absence of dolabralexins in the maize *Zman2* mutant.

Supplemental Figure S8. LC-MS/MS spectra of trihydroxydolabrene.

Supplemental Figure S9. Routine analysis of trihydroxydolabrene.

Supplemental Figure S10. NMR elucidation of trihydroxydolabrene.

Supplemental Table S1. Oligonucleotides and plasmid constructs used in this study.

Supplemental Table S2. Protein sequences used in phylogenetic analyses.

ACKNOWLEDGMENTS

We thank Dr. David Nelson (University of Tennessee) for assistance with the annotation of ZmCYP71Z16 and Dr. Reuben Peters (Iowa State University) for providing the pIRS, pGGxC, and *ZmAN2* constructs and select authentic standards.

Received September 19, 2017; accepted February 16, 2018; published February 23, 2018.

LITERATURE CITED

Ahmad S, Veyrat N, Gordon-Weeks R, Zhang Y, Martin J, Smart L, Glauser G, Erb M, Flors V, Frey M, et al (2011) Benzoxazinoid metabolites regulate innate immunity against aphids and fungi in maize. Plant Physiol **157:** 317–327

Baldwin TT, Zitomer NC, Mitchell TR, Zimeri AM, Bacon CW, Riley RT, Glenn AE (2014) Maize seedling blight induced by Fusarium verticillioides: accumulation of fumonisin B_1 in leaves without colonization of the leaves. J Agric Food Chem **62:** 2118–2125

Bensen RJ, Johal GS, Crane VC, Tossberg JT, Schnable PS, Meeley RB, Briggs SP (1995) Cloning and characterization of the maize An1 gene. Plant Cell **7:** 75–84

Brophy JJ, Goldsack RJ, Wu MZ, Fookes CJ, Forster PI (2000) The steam volatile oil of *Wollemia nobilis* and its comparison with other members of the Araucariaceae (*Agathis* and *Araucaria*). Biochem Syst Ecol **28:** 563–578

Brückner K, Tissier A (2013) High-level diterpene production by transient expression in *Nicotiana benthamiana*. Plant Methods **9:** 46

Chakraborty S, Newton AC (2011) Climate change, plant diseases and food security: an overview. Plant Pathol **60:** 2–14

Chaturvedi R, Venables B, Petros RA, Nalam V, Li M, Wang X, Takemoto LJ, Shah J (2012) An abietane diterpenoid is a potent activator of systemic acquired resistance. Plant J **71:** 161–172

Chourey K, Jansson J, VerBerkmoes N, Shah M, Chavarria KL, Tom LM, Brodie EL, Hettich RL (2010) Direct cellular lysis/protein extraction protocol for soil metaproteomics. J Proteome Res **9:** 6615–6622

Christensen SA, Huffaker A, Kaplan F, Sims J, Ziemann S, Doehlemann G, Ji L, Schmitz RJ, Kolomiets MV, Alborn HT, et al (2015) Maize death acids, 9-lipoxygenase-derived cyclopente(a)nones, display activity as cytotoxic phytoalexins and transcriptional mediators. Proc Natl Acad Sci USA **112:** 11407–11412

Christensen SA, Sims J, Vaughan M, Hunter C, Block A, Willett D, Alborn HT, Huffaker A, Schmelz EA (2018) Commercial hybrids and mutant genotypes reveal complex protective roles for inducible terpenoid defenses. J Exp Bot doi.org/10.1093/jxb/erx495

Christie N, Myburg AA, Joubert F, Murray SL, Carstens M, Lin YC, Meyer J, Crampton BG, Christensen SA, Ntuli JF, et al (2017) Systems genetics reveals a transcriptional network associated with susceptibility in the maize-grey leaf spot pathosystem. Plant J **89:** 746–763

Cui G, Duan L, Jin B, Qian J, Xue Z, Shen G, Snyder JH, Song J, Chen S, Huang L, et al (2015) Functional divergence of diterpene syntheses in the medicinal plant *Salvia miltiorrhiza*. Plant Physiol **169:** 1607–1618

Degenhardt J (2009) Indirect defense responses to herbivory in grasses. Plant Physiol **149:** 96–102

Degenhardt J, Hiltpold I, Köllner TG, Frey M, Gierl A, Gershenzon J, Hibbard BE, Ellersieck MR, Turlings TCJ (2009) Restoring a maize root signal that attracts insect-killing nematodes to control a major pest. Proc Natl Acad Sci USA **106:** 13213–13218

de Sassi C, Tylianakis JM (2012) Climate change disproportionately increases herbivore over plant or parasitoid biomass. PLoS ONE **7:** e40557

Ding Y, Huffaker A, Köllner TG, Weckwerth P, Robert CAM, Spencer JL, Lipka AE, Schmelz EA (2017) Selinene volatiles are essential precursors for maize defense promoting fungal pathogen resistance. Plant Physiol **175:** 1455–1468

Fu J, Ren F, Lu X, Mao H, Xu M, Degenhardt J, Peters RJ, Wang Q (2016) A tandem array of *ent*-kaurene synthases in maize with roles in gibberellin and more specialized metabolism. Plant Physiol **170:** 742–751

Gershenzon J, Dudareva N (2007) The function of terpene natural products in the natural world. Nat Chem Biol **3:** 408–414

Goswami RS, Kistler HC (2004) Heading for disaster: *Fusarium graminearum* on cereal crops. Mol Plant Pathol **5:** 515–525

Grass Phylogeny Working Group II (2012) New grass phylogeny resolves deep evolutionary relationships and discovers C4 origins. New Phytol **193:** 304–312

Guindon S, Dufayard JF, Lefort V, Anisimova M, Hordijk W, Gascuel O (2010) New algorithms and methods to estimate maximum-likelihood phylogenies: assessing the performance of PhyML 3.0. Syst Biol **59:** 307–321

Hall DE, Zerbe P, Jancsik S, Quesada AL, Dullat H, Madilao LL, Yuen M, Bohlmann J (2013) Evolution of conifer diterpene synthases: diterpene resin acid biosynthesis in lodgepole pine and jack pine involves monofunctional and bifunctional diterpene synthases. Plant Physiol **161:** 600–616

Hamberger B, Bak S (2013) Plant P450s as versatile drivers for evolution of species-specific chemical diversity. Philos Trans R Soc Lond B Biol Sci **368:** 20120426

Harris LJ, Saparno A, Johnston A, Prisic S, Xu M, Allard S, Kathiresan A, Ouellet T, Peters RJ (2005) The maize An2 gene is induced by *Fusarium* attack and encodes an *ent*-copalyl diphosphate synthase. Plant Mol Biol **59:** 881–894

Hartmann T (2007) From waste products to ecochemicals: fifty years research of plant secondary metabolism. Phytochemistry **68:** 2831–2846

Hedden P, Sponsel V (2015) A century of gibberellin research. J Plant Growth Regul **34:** 740–760

Huffaker A, Kaplan F, Vaughan MM, Dafoe NJ, Ni X, Rocca JR, Alborn HT, Teal PE, Schmelz EA (2011) Novel acidic sesquiterpenoids constitute a dominant class of pathogen-induced phytoalexins in maize. Plant Physiol **156:** 2082–2097

Jensen NB, Zagrobelny M, Hjernø K, Olsen CE, Houghton-Larsen J, Borch J, Møller BL, Bak S (2011) Convergent evolution in biosynthesis of cyanogenic defence compounds in plants and insects. Nat Commun **2:** 273

Kato-Noguchi H, Kobayashi K (2009) Jasmonic acid, protein phosphatase inhibitor, metals and UV-irradiation increased momilactone A and B concentrations in the moss *Hypnum plumaeforme*. J Plant Physiol **166:** 1118–1122

Kato-Noguchi H, Peters RJ (2013) The role of momilactones in rice allelopathy. J Chem Ecol **39:** 175–185

Keeling CI, Bohlmann J (2006) Diterpene resin acids in conifers. Phytochemistry **67:** 2415–2423

Kitaoka N, Lu X, Yang B, Peters RJ (2015) The application of synthetic biology to elucidation of plant mono-, sesqui-, and diterpenoid metabolism. Mol Plant **8:** 6–16

Köllner TG, Held M, Lenk C, Hiltpold I, Turlings TC, Gershenzon J, Degenhardt J (2008a) A maize (E)-beta-caryophyllene synthase implicated in indirect defense responses against herbivores is not expressed in most American maize varieties. Plant Cell **20:** 482–494

Köllner TG, Schnee C, Li S, Svatos A, Schneider B, Gershenzon J, Degenhardt J (2008b) Protonation of a neutral (S)-beta-bisabolene intermediate is involved in (S)-beta-macrocarpene formation by the maize sesquiterpene synthases TPS6 and TPS11. J Biol Chem **283:** 20779–20788

Kolosova N, Miller B, Ralph S, Ellis BE, Douglas C, Ritland K, Bohlmann J (2004) Isolation of high-quality RNA from gymnosperm and angiosperm trees. Biotechniques **36:** 821–824

Lange BM, Ahkami A (2013) Metabolic engineering of plant monoterpenes, sesquiterpenes and diterpenes: current status and future opportunities. Plant Biotechnol J **11:** 169–196

Mao H, Liu J, Ren F, Peters RJ, Wang Q (2016) Characterization of CYP71Z18 indicates a role in maize zealexin biosynthesis. Phytochemistry **121:** 4–10

Mao H, Shen Q, Wang Q (2017) CYP701A26 is characterized as an *ent*-kaurene oxidase with putative involvement in maize gibberellin biosynthesis. Biotechnol Lett **39:** 1709–1716

Matsuba Y, Nguyen TT, Wiegert K, Falara V, Gonzales-Vigil E, Leong B, Schäfer P, Kudrna D, Wing RA, Bolger AM, et al (2013) Evolution of a complex locus for terpene biosynthesis in *Solanum*. Plant Cell **25:** 2022–2036

Morrone D, Hillwig ML, Mead ME, Lowry L, Fulton DB, Peters RJ (2011) Evident and latent plasticity across the rice diterpene synthase family with potential implications for the evolution of diterpenoid metabolism in the cereals. Biochem J **435:** 589–595

Morrone D, Jin Y, Xu M, Choi SY, Coates RM, Peters RJ (2006) An unexpected diterpene cyclase from rice: functional identification of a stemodene synthase. Arch Biochem Biophys **448:** 133–140

Morrone D, Lowry L, Determan MK, Hershey DM, Xu M, Peters RJ (2010) Increasing diterpene yield with a modular metabolic engineering system in *E. coli*: comparison of MEV and MEP isoprenoid precursor pathway engineering. Appl Microbiol Biotechnol **85:** 1893–1906

Munkvold GA (1997) Fumonisins in maize: can we reduce their occurrence? Plant Dis **81:** 556–565

Munné-Bosch S, Alegre L (2000) Changes in carotenoids, tocopherols and diterpenes during drought and recovery, and the biological significance of chlorophyll loss in *Rosmarinus officinalis* plants. Planta **210:** 925–931

Nützmann HW, Huang A, Osbourn A (2016) Plant metabolic clusters: from genetics to genomics. New Phytol **211:** 771–789

Peters RJ (2006) Uncovering the complex metabolic network underlying diterpenoid phytoalexin biosynthesis in rice and other cereal crop plants. Phytochemistry **67:** 2307–2317

Peters RJ (2010) Two rings in them all: the labdane-related diterpenoids. Nat Prod Rep **27:** 1521–1530

Peters RJ, Croteau RB (2002) Abietadiene synthase catalysis: mutational analysis of a prenyl diphosphate ionization-initiated cyclization and rearrangement. Proc Natl Acad Sci USA **99:** 580–584

Pichersky E, Gershenzon J (2002) The formation and function of plant volatiles: perfumes for pollinator attraction and defense. Curr Opin Plant Biol **5:** 237–243

Pichersky E, Lewinsohn E (2011) Convergent evolution in plant specialized metabolism. Annu Rev Plant Biol **62:** 549–566

Pompon D, Louerat B, Bronine A, Urban P (1996) Yeast expression of animal and plant P450s in optimized redox environments. Methods Enzymol **272:** 51–64

Prisic S, Xu M, Wilderman PR, Peters RJ (2004) Rice contains two disparate *ent*-copalyl diphosphate synthases with distinct metabolic functions. Plant Physiol **136:** 4228–4236

Rahman H, Pekic S, Lazic-Jancic V, Quarrie SA, Shah SM, Pervez A, Shah MM (2011) Molecular mapping of quantitative trait loci for drought tolerance in maize plants. Genet Mol Res **10:** 889–901

Richter A, Schaff C, Zhang Z, Lipka AE, Tian F, Köllner TG, Schnee C, Preiß S, Irmisch S, Jander G, et al (2016) Characterization of biosynthetic pathways for the production of the volatile homoterpenes DMNT and TMTT in *Zea mays*. Plant Cell **28:** 2651–2665

Richter A, Seidl-Adams I, Köllner TG, Schaff C, Tumlinson JH, Degenhardt J (2015) A small, differentially regulated family of farnesyl diphosphate synthases in maize (*Zea mays*) provides farnesyl diphosphate for the biosynthesis of herbivore-induced sesquiterpenes. Planta **241:** 1351–1361

Santiago R, Malvar RA (2010) Role of dehydrodiferulates in maize resistance to pests and diseases. Int J Mol Sci **11:** 691–703

Schmelz EA, Alborn HT, Tumlinson JH (2001) The influence of intact-plant and excised-leaf bioassay designs on volicitin- and jasmonic acid-induced sesquiterpene volatile release in *Zea mays*. Planta **214:** 171–179

Schmelz EA, Engelberth J, Alborn HT, Tumlinson JH III, Teal PE (2009) Phytohormone-based activity mapping of insect herbivore-produced elicitors. Proc Natl Acad Sci USA **106:** 653–657

Schmelz EA, Engelberth J, Tumlinson JH, Block A, Alborn HT (2004) The use of vapor phase extraction in metabolic profiling of phytohormones and other metabolites. Plant J **39:** 790–808

Schmelz EA, Huffaker A, Sims JW, Christensen SA, Lu X, Okada K, Peters RJ (2014) Biosynthesis, elicitation and roles of monocot terpenoid phytoalexins. Plant J **79:** 659–678

Schmelz EA, Kaplan F, Huffaker A, Dafoe NJ, Vaughan MM, Ni X, Rocca JR, Alborn HT, Teal PE (2011) Identity, regulation, and activity of inducible diterpenoid phytoalexins in maize. Proc Natl Acad Sci USA **108:** 5455–5460

Schnee C, Köllner TG, Held M, Turlings TC, Gershenzon J, Degenhardt J (2006) The products of a single maize sesquiterpene synthase form a volatile defense signal that attracts natural enemies of maize herbivores. Proc Natl Acad Sci USA **103:** 1129–1134

Swaminathan S, Morrone D, Wang Q, Fulton DB, Peters RJ (2009) CYP76M7 is an *ent*-cassadiene C11alpha-hydroxylase defining a second multifunctional diterpenoid biosynthetic gene cluster in rice. Plant Cell **21:** 3315–3325

Takahashi K, Nagahama S, Nakashima T, Suenaga H (2001) Chemotaxonomy on the leaf constituents of *Thujopsis dolabrata* Sieb. et Zucc.: analysis of neutral extracts (diterpene hydrocarbon). Biochem Syst Ecol **29:** 839–848

Talavera G, Castresana J (2007) Improvement of phylogenies after removing divergent and ambiguously aligned blocks from protein sequence alignments. Syst Biol **56:** 564–577

Tholl D (2015) Biosynthesis and biological functions of terpenoids in plants. Adv Biochem Eng Biotechnol **148:** 63–106

Toyomasu T, Kagahara T, Okada K, Koga J, Hasegawa M, Mitsuhashi W, Sassa T, Yamane H (2008) Diterpene phytoalexins are biosynthesized in and exuded from the roots of rice seedlings. Biosci Biotechnol Biochem **72:** 562–567

Toyomasu T, Usui M, Sugawara C, Otomo K, Hirose Y, Miyao A, Hirochika H, Okada K, Shimizu T, Koga J, et al (2014) Reverse-genetic approach to verify physiological roles of rice phytoalexins: characterization of a knockdown mutant of OsCPS4 phytoalexin biosynthetic gene in rice. Physiol Plant **150:** 55–62

Tuberosa R, Salvi S, Sanguineti MC, Landi P, Maccaferri M, Conti S (2002) Mapping QTLs regulating morpho-physiological traits and yield: case studies, shortcomings and perspectives in drought-stressed maize. Ann Bot **89:** 941–963

van der Linde K, Kastner C, Kumlehn J, Kahmann R, Doehlemann G (2011) Systemic virus-induced gene silencing allows functional characterization of maize genes during biotrophic interaction with *Ustilago maydis*. New Phytol **189:** 471–483

Vaughan MM, Christensen S, Schmelz EA, Huffaker A, McAuslane HJ, Alborn HT, Romero M, Allen LH, Teal PE (2015) Accumulation of terpenoid phytoalexins in maize roots is associated with drought tolerance. Plant Cell Environ **38:** 2195–2207

Vaughan MM, Huffaker A, Schmelz EA, Dafoe NJ, Christensen S, Sims J, Martins VF, Swerbilow J, Romero M, Alborn HT, et al (2014) Effects of elevated [CO_2] on maize defence against mycotoxigenic *Fusarium verticillioides*. Plant Cell Environ **37:** 2691–2706

Vaughan MM, Wang Q, Webster FX, Kiemle D, Hong YJ, Tantillo DJ, Coates RM, Wray AT, Askew W, O'Donnell C, et al (2013) Formation of the unusual semivolatile diterpene rhizathalene by the *Arabidopsis* class I terpene synthase TPS08 in the root stele is involved in defense against belowground herbivory. Plant Cell **25:** 1108–1125

Wang Q, Hillwig ML, Okada K, Yamazaki K, Wu Y, Swaminathan S, Yamane H, Peters RJ (2012a) Characterization of CYP76M5-8 indicates metabolic plasticity within a plant biosynthetic gene cluster. J Biol Chem **287:** 6159–6168

Wang Q, Hillwig ML, Peters RJ (2011) CYP99A3: functional identification of a diterpene oxidase from the momilactone biosynthetic gene cluster in rice. Plant J **65:** 87–95

Wang Q, Hillwig ML, Wu Y, Peters RJ (2012b) CYP701A8: a rice *ent*-kaurene oxidase paralog diverted to more specialized diterpenoid metabolism. Plant Physiol **158:** 1418–1425

Wolfe KH, Gouy M, Yang YW, Sharp PM, Li WH (1989) Date of the monocot-dicot divergence estimated from chloroplast DNA sequence data. Proc Natl Acad Sci USA **86:** 6201–6205

Wouters FC, Blanchette B, Gershenzon J, Vassão DG (2016) Plant defense and herbivore counter-defense: benzoxazinoids and insect herbivores. Phytochem Rev **15:** 1127–1151

Wu Y, Hillwig ML, Wang Q, Peters RJ (2011) Parsing a multifunctional biosynthetic gene cluster from rice: biochemical characterization of CYP71Z6 & 7. FEBS Lett **585:** 3446–3451

Wu Y, Zhou K, Toyomasu T, Sugawara C, Oku M, Abe S, Usui M, Mitsuhashi W, Chono M, Chandler PM, et al (2012) Functional characterization of wheat copalyl diphosphate synthases sheds light on the early evolution of labdane-related diterpenoid metabolism in the cereals. Phytochemistry **84:** 40–46

Xu M, Hillwig ML, Prisic S, Coates RM, Peters RJ (2004) Functional identification of rice *syn*-copalyl diphosphate synthase and its role in initiating biosynthesis of diterpenoid phytoalexin/allelopathic natural products. Plant J **39:** 309–318

Xu M, Wilderman PR, Morrone D, Xu J, Roy A, Margis-Pinheiro M, Upadhyaya NM, Coates RM, Peters RJ (2007a) Functional characterization of the rice kaurene synthase-like gene family. Phytochemistry **68:** 312–326

Xu M, Wilderman PR, Peters RJ (2007b) Following evolution's lead to a single residue switch for diterpene synthase product outcome. Proc Natl Acad Sci USA **104:** 7397–7401

Zerbe P, Bohlmann J (2015) Plant diterpene synthases: exploring modularity and metabolic diversity for bioengineering. Trends Biotechnol **33:** 419–428

Zerbe P, Hamberger B, Yuen MM, Chiang A, Sandhu HK, Madilao LL, Nguyen A, Hamberger B, Bach SS, Bohlmann J (2013) Gene discovery of modular diterpene metabolism in nonmodel systems. Plant Physiol **162:** 1073–1091

Zhou K, Xu M, Tiernan M, Xie Q, Toyomasu T, Sugawara C, Oku M, Usui M, Mitsuhashi W, Chono M, et al (2012) Functional characterization of wheat *ent*-kaurene(-like) synthases indicates continuing evolution of labdane-related diterpenoid metabolism in the cereals. Phytochemistry **84:** 47–55

Zi J, Mafu S, Peters RJ (2014) To gibberellins and beyond! Surveying the evolution of (di)terpenoid metabolism. Annu Rev Plant Biol **65:** 259–286

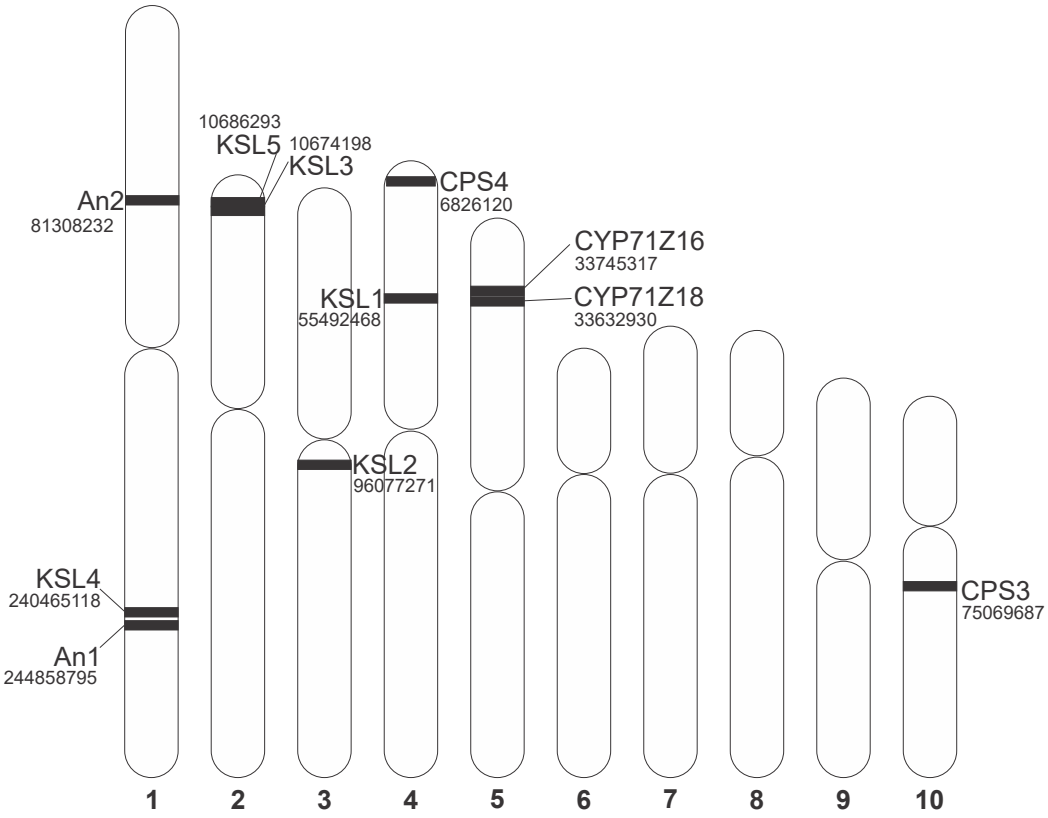

Supplemental Fig. S1: Chromosomal location of maize diTPS and P450 genes.

Supplemental Fig. S2: NMR analysis of dolabradiene.

(A) Proton chemical shifts ^{1}H NMR, (800 MHz chloroform-*d,* 303.3 K), δ (ppm): 1.68 (1H, m, H1a), 1.44 (1H, m, H1b), 1.9 (1H, m, H2a), 1.3 (1H, m, H2b), 2.32 (1H, tdt, J=13.7, 5.2, 1.6 Hz, H3a), 2.12 (1H, ddt, J=13.5, 4.2, 1.8 Hz, H3b), 1.66 (2H, m, H6), 1.46 (1H, m, H7a), 1.25 (1H, dq=13.4, 3.4 Hz, H7b), 1.32 (1H, m, H8), 0.95 (1H, dd, J=12.5, 2.8 Hz, H10), 1.56 (1H, m, H11a), 1.05 (1H, td, J=16.0, 15.2, 4.6 Hz, H11b) 1.57 (1H, m, H12a), 1.21 (1H, m, H12b), 1.37 (1H, q, J=14.0, 13.5 Hz, H14a), 0.99 (1H, dt, J=12.8, 2.5 Hz, H14b), 5.83 (1H, dd, J=17.5, 10.7 Hz, H15), 4.93 (1H, dd, J=17.5, 1.4 Hz, H16a), 4.86 (1H, dd, J=10.7, 1.4 Hz, H16b), 1.02 (3H, s, H17), 4.52 (2H, dt, J=15.7, 1.8 Hz, H18), 1.09 (3H, s, H19), 0.78 (3H, s, H_20).

Carbon chemical shifts, (2.01 MHz, chloroform-d, 303.3 K) and assignments were as follows: δ (ppm). 21.18 (C1), 28.78 (C2), 33.17 (C3), 160.93 (C4), 40.69 (C5), 37.95 (C6), 26.05 (C7), 42.45 (C8), 37.36 (C9), 56.43 (C10), 35.27 (C11), 32.10 (C12), 36.42 (C13), 39.23 (C14), 151.47 (C15), 108.54 (C16), 23.06 (C17), 102.01 (C18), 21.60 (C19), 12.42 (C20).

(B) Dolabradiene numbering and correlations

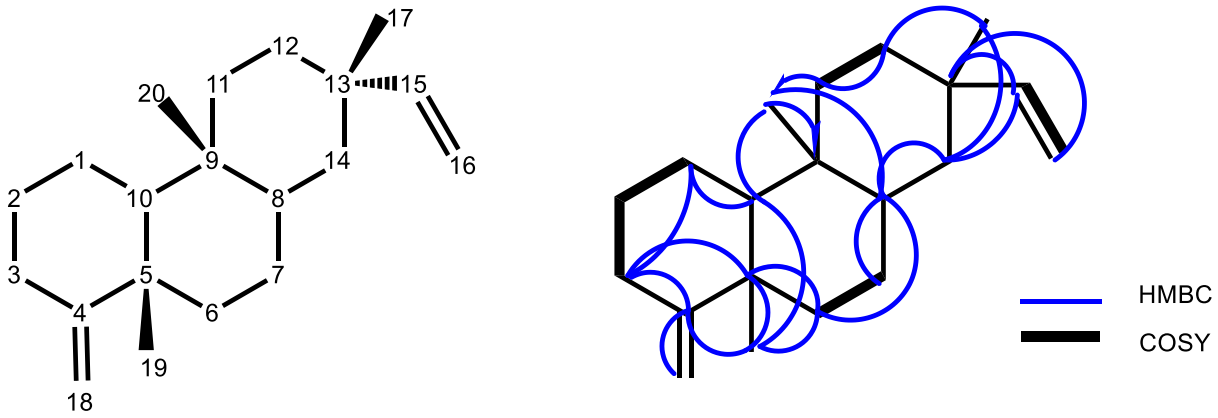

Supplemental Fig. S2, continued

(C) ^{1}H spectrum of dolabradiene.

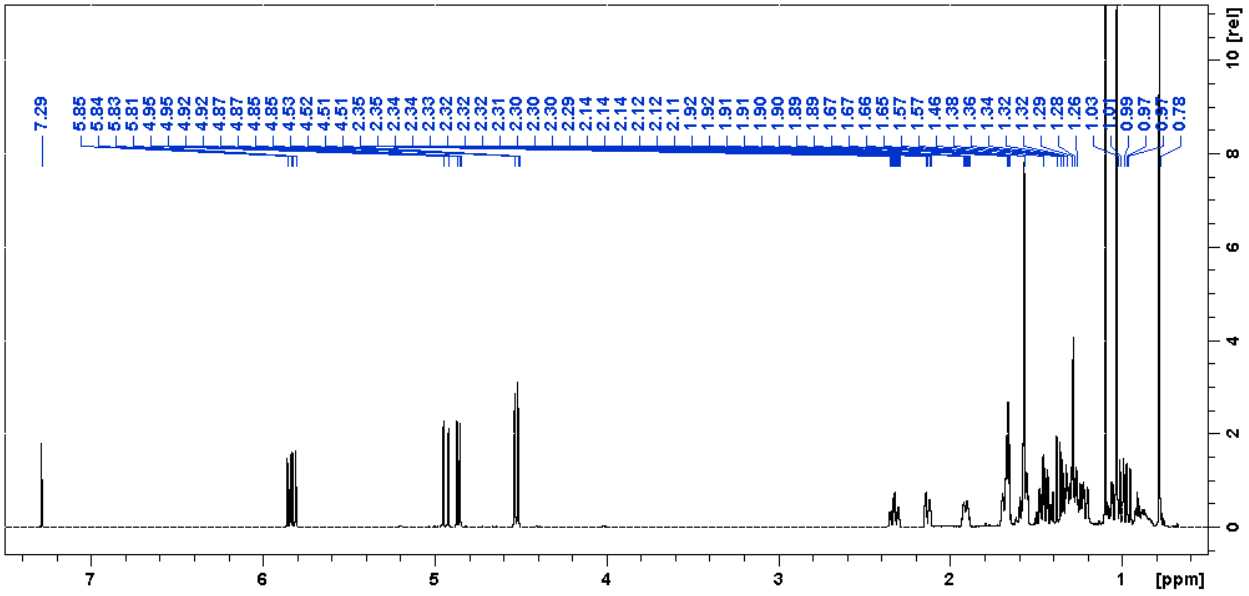

(D) ^{13}C spectrum of dolabradiene.

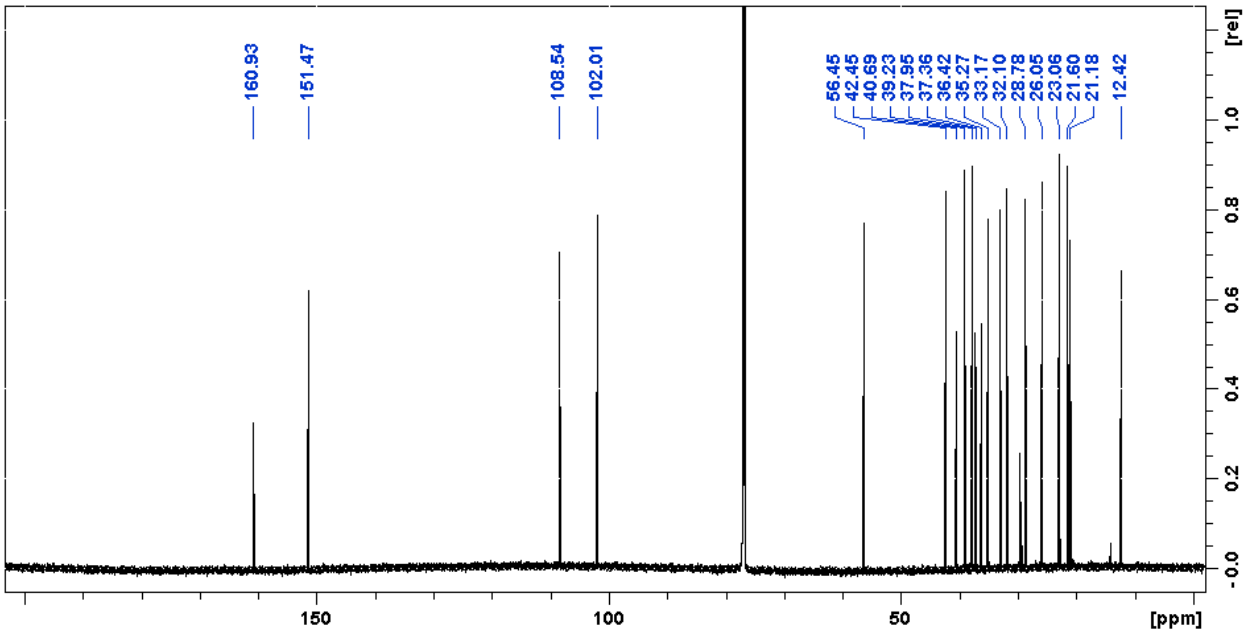

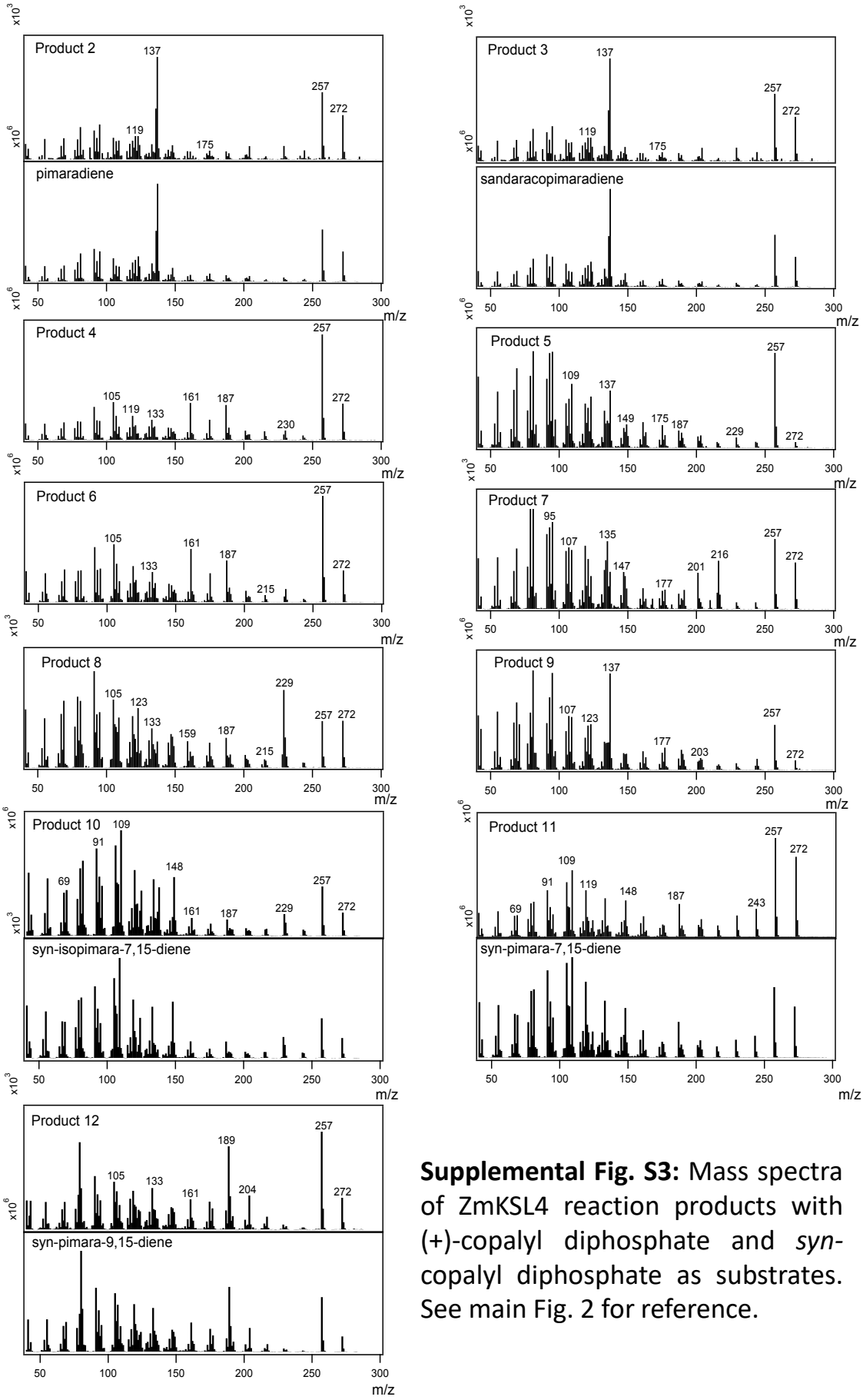

Supplemental Fig. S3: Mass spectra of ZmKSL4 reaction products with (+)-copalyl diphosphate and *syn*-copalyl diphosphate as substrates. See main Fig. 2 for reference.

Supplemental Fig. S4: NMR analysis of the CYP71Z16 reaction products.

(A) 15,16-epoxydolbrene proton chemical shifts 1H NMR, (800 MHz chloroform-*d,* 298 K), δ (ppm): 1.65 (1H, m, H1a), 1.41 (1H, m, H1b), 1.88 (1H, m, H2a), 1.27 (1H, m, H2b), 2.29 (1H, m, 3a), 2.10 (1H, dt, J=13.62, 2.15, 2.15 Hz, H3b), 1.63 (2H, m, H6), 1.2 (1H, m, H7a), 1.4 (1H, m, H7b), 1.26 (1H, m, H8), 0.91 (1H, m, H10), 1.56 (1H, m, H11a), 1.02 (1H, td, J=13.62, 13.62, 4.04 Hz, H11b), 1.62 (1H, m, H12a), 1.24 (1H, m H12b), 1.26 (1H, m, H14a), 0.83 (1H, br d, J=7.78, H14b), 2.69 (1H,t, J=3.48 Hz, H15), 2.66 (1H, dd, J=4.48, 3.11Hz, H16a), 2.64 (lH, t, J=4.40 Hz, H16b), 0.93 (3H,s), 4.50 (2H,d, J=11.76 Hz, H18), 1.06 (3H,s), 0.75 (3H,s).

Carbon chemical shifts, (2.01 MHz, chloroform-d, 298 K) and assignments were as follows: δ (ppm). 21.17 (C1), 28.75 (C2), 33.13 (C3), 160.84 (C4), 40.64 (C5), 37.88 (C6), 26.08 (C7), 41.92 (C8), 37.38 (C9), 56.35 (C10), 34.80 (C11), 29.61 (C12), 33.42(C13), 34.25 (C14), 61.07 (C15), 43.51 (C16), 20.51 (C17), 102.03 (C18), 21.55 (C19), 12.31 (C20)

(B) 15,16-epoxydolabrene numbering and correlations.

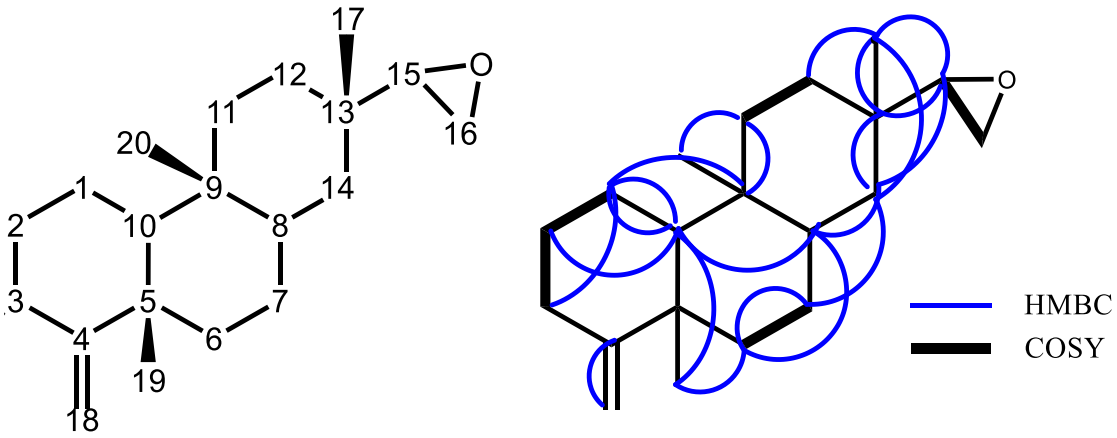

Supplemental Fig. S4, continued

(C) ^{1}H spectrum of 15,16-epoxydolabrene.

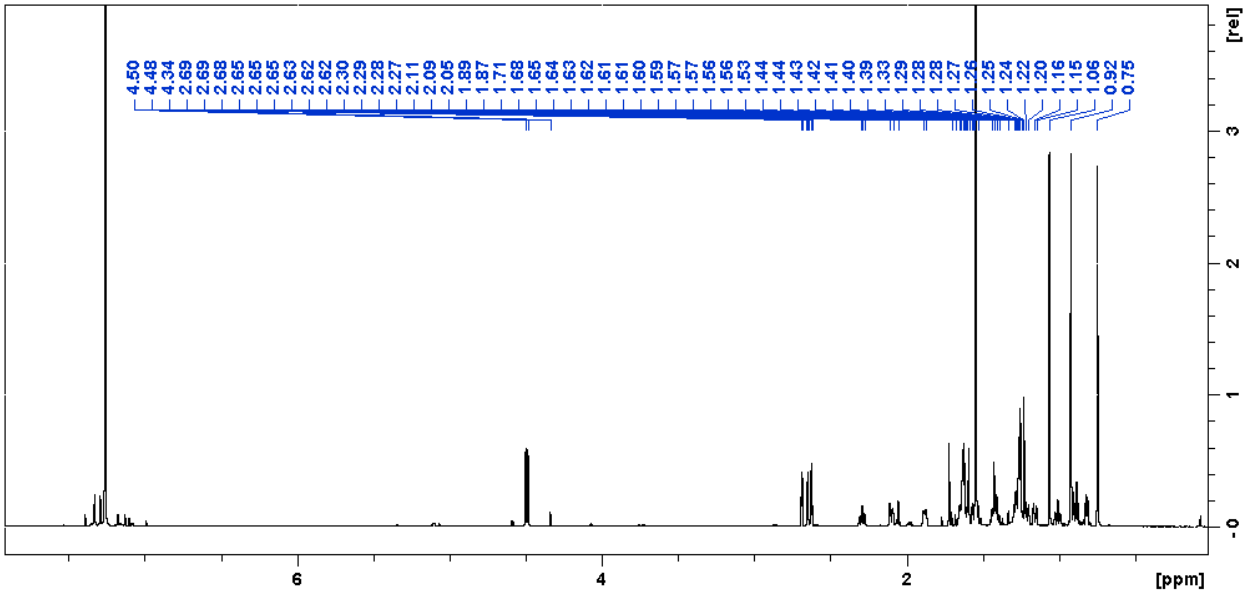

(D) ^{13}C spectrum of 15,16-epoxydolabrene.

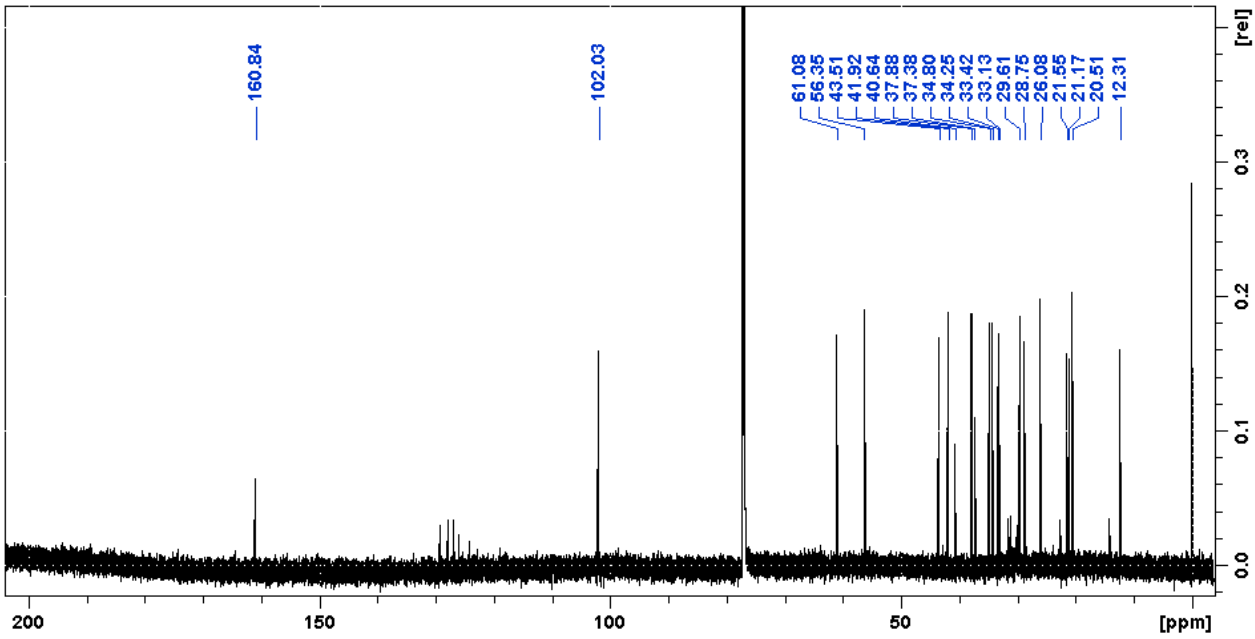

Supplemental Fig. S4, continued

(E) NMR analysis of 3β-hydroxy-15,16-epoxydolabrene proton chemical shifts ^{1}H NMR (800 MHz chloroform-*d,* 298 K): δ (ppm): 1.76 (1H,m, H1a), 1.55 (1H, br d, 1.47 Hz, H1b), 2.02 (1H, m, H2a), 1.56 (1H, m, H2b), 4.33 (1H, t, J=2.93, H3), 1.74 (1H, dq, 9.35, 3.04, 3.04 3.04 H6a), 1.53 (1H, m, H6b), 1.45 (1H, m, H7a), 1.20 (1H, m, H7b), 1.25 (1H, m, H8), 0.92 (1H, m, H10), 1.62 (1H, m, H11a), 1.02 (1H, dd, J=10.12, 2.05 Hz,H11b), 1.65 (1H, m, H12a), 1.18 (1H, m, H12b), 1.26 (1H, m, H14a), 0.83 (1H, dd, J=10.16, 2.16 Hz, H14b), 2.69 (1H, dd, J= 4.00, 3.4 Hz, H15), 2.66 (1H, dd, J= 4.72, 2.96, H16a), 2.64 (1H, t, J=4.40Hz, H16b), 0.92 (3H, s, H17), 4.82 (2H, dd, J=43.87, J=1.00 Hz, H18), 1.25 (3H, s, H19), 0.79 (3H, s, H19);

Carbon chemical shifts (2.01 MHz, chloroform-d, 298 K) and assignments were as follows: δ (ppm). 16.21 (C1), 34.86 (C2), 74.78 (C3), 160.98 (C4), 40.35 (C5), 38.73 (C6), 25.64 (C7), 41.89 (C8), 37.35 (C9), 56.33 (C10), 34.87 (C11), 29.57 (C12), 33.41 (C13), 34.28 (C14), 60.96 (C15), 43.61 (C16), 20.45 (C17), 109.13 (C18), 23.67 (C19), 12.33 (C20)

(F) Numbering and correlations of 3β-hydroxy-15,16-epoxydolabrene.

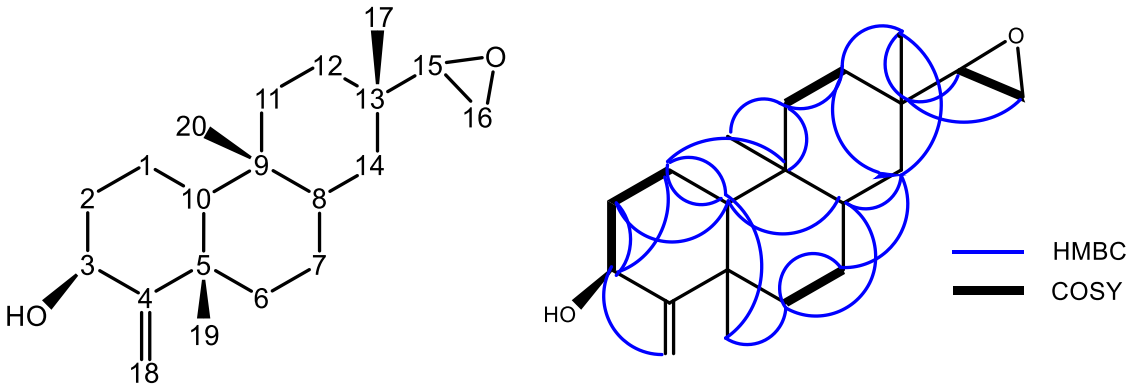

Supplemental Fig. S4, continued

(G) ^{1}H spectrum of 3β-hydroxy-15,16-epoxydolabrene.

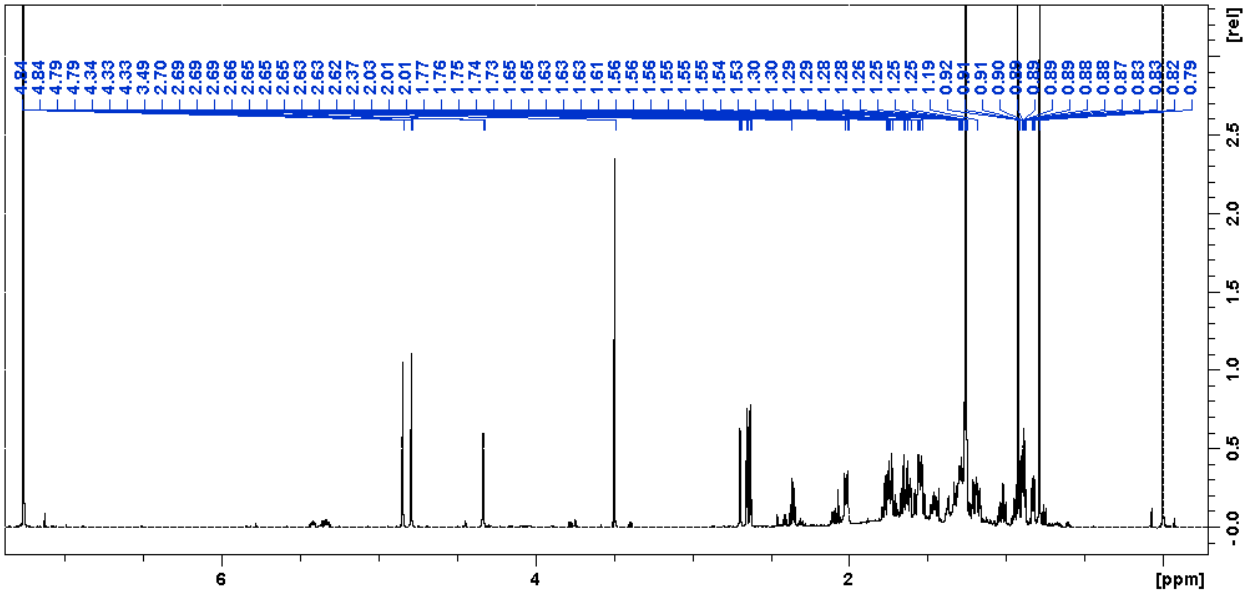

(H) ^{13}C spectrum of 3β-hydroxy-15,16-epoxydolabrene.

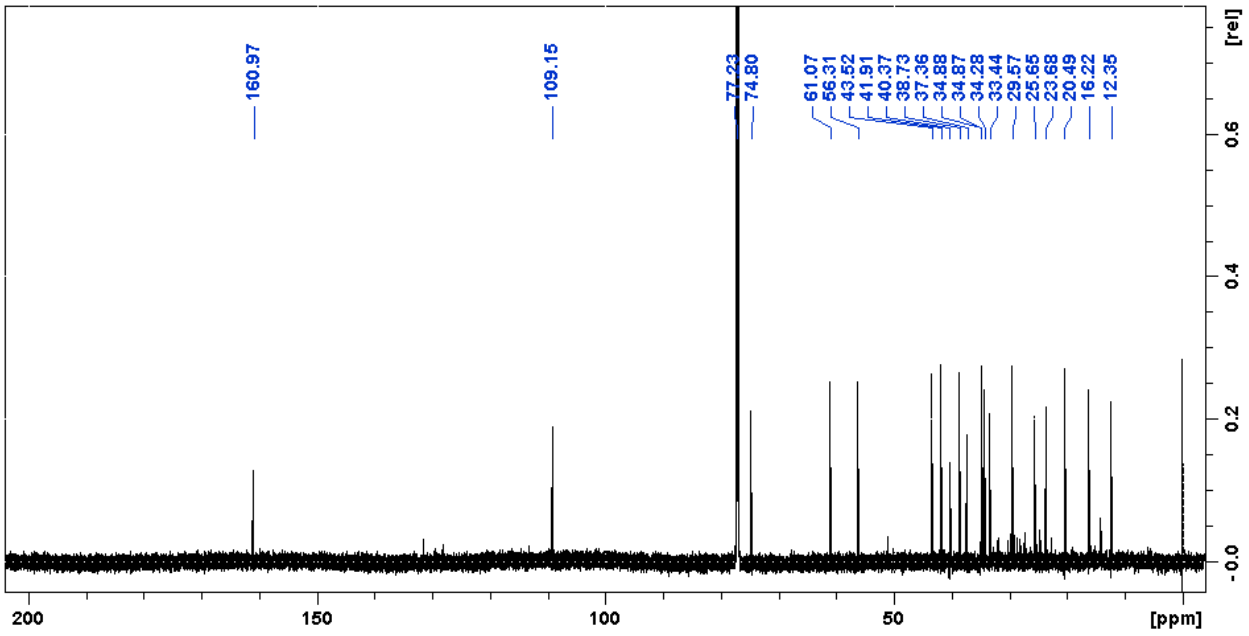

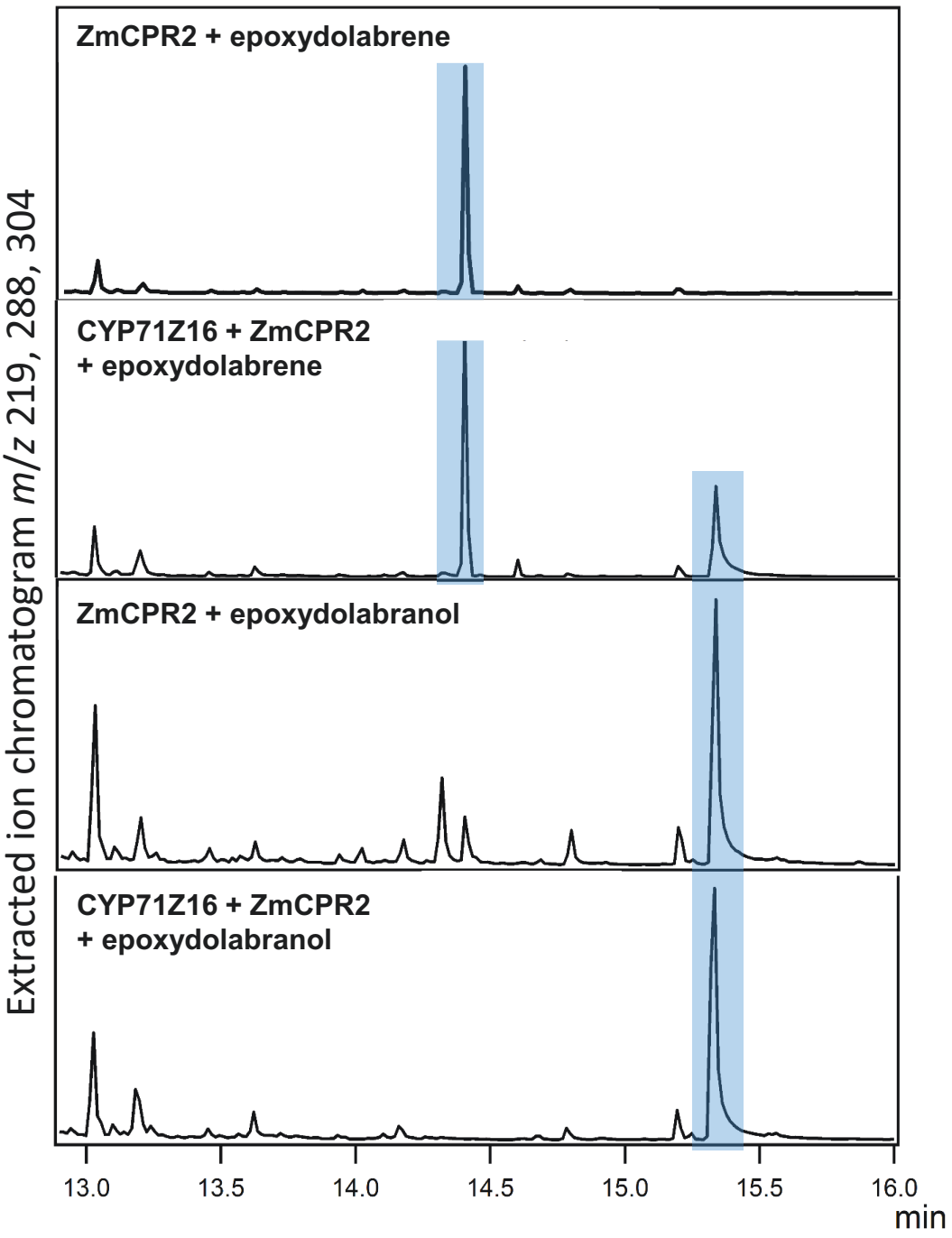

Supplemental Fig. S5: Feeding assays of CYP71Z16.

Total ion chromatograms depicting reaction products resulting from whole cell *E. coli* co-expression assays after feeding of purified epoxydolabrene **13** and epoxydolabranol **14** to the culture medium. Feeding of epoxydolabranol to cultures expressing ZmCPR2 alone were used as a control.

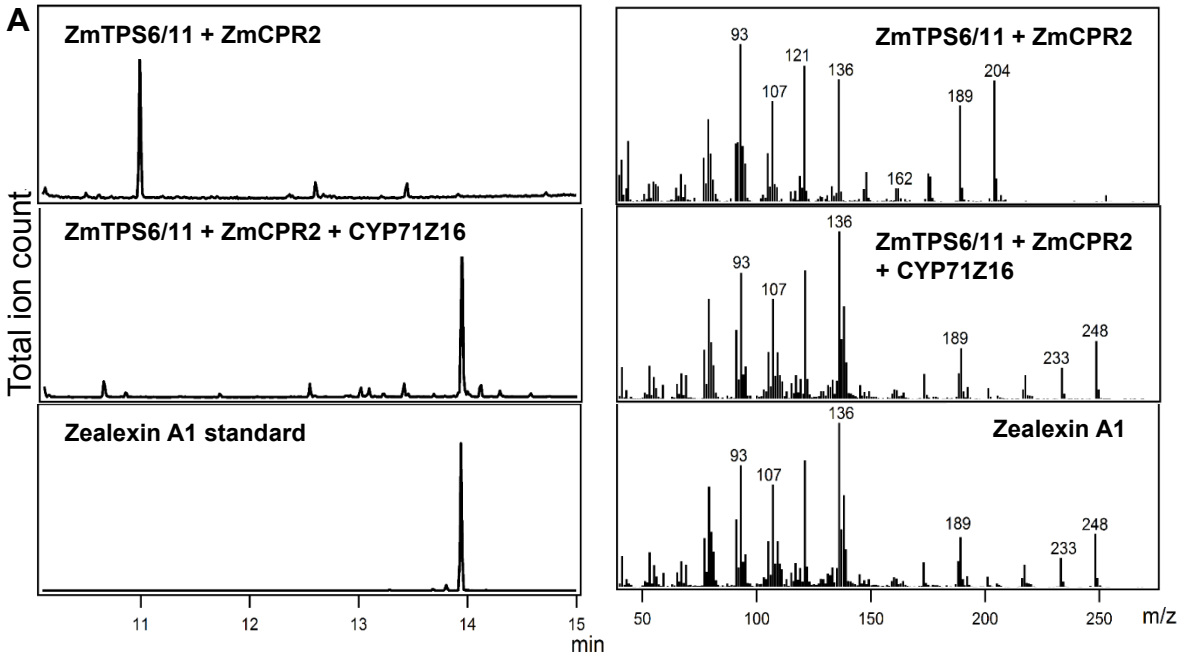

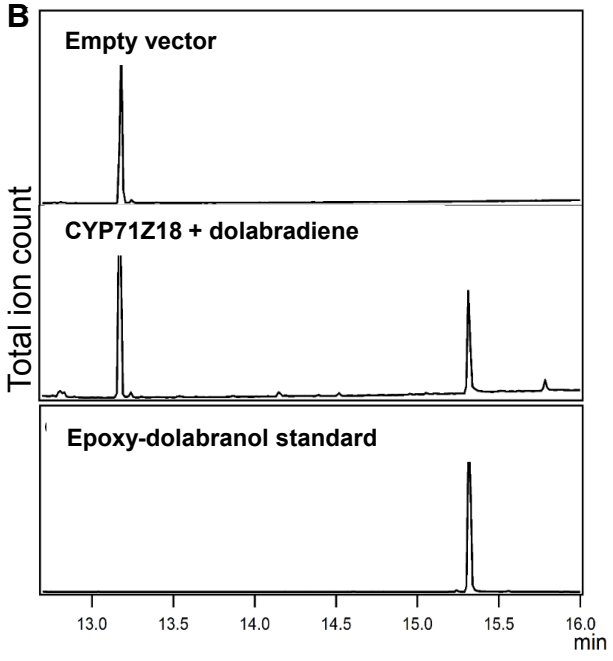

Supplemental Fig. S6: Substrate specificity of CYP71Z16 and CYP71Z18.

(**A**)Total ion chromatograms (TIC) and mass spectra of reaction products derived from *E.coli* co-expression assays with ZmTPS6/11, ZmCPR2 and CYP71Z16 as compared to authentic zealexin A1 as a standard. (**B**) TICs of reaction products derived from yeast (*S. cerevisiae*, strain BY4741) expression of CYP71Z18 with feeding of 25 μM purified dolabradiene.

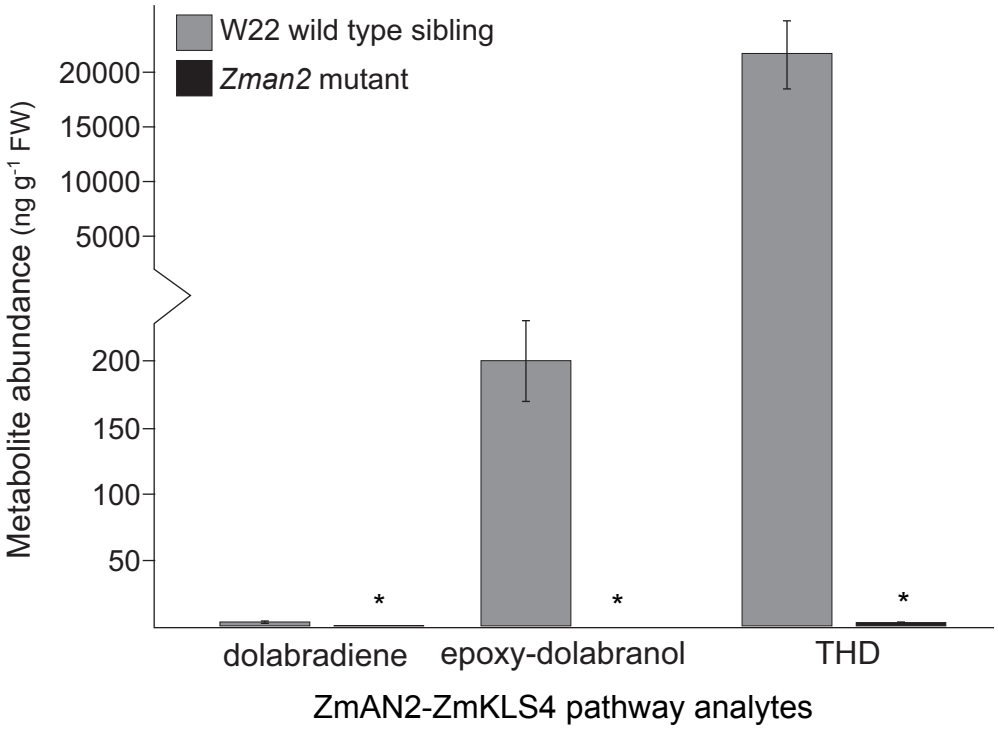

Supplemental Figure S7: Absence of dolabralexins in the maize *Zman2* mutant. Average (*n* =4; ± SEM) quantities of dolabradiene, epoxy-dolabranol and the 3β,15,16-trihydroxydolabradiene (THD) in 16-day old seedling roots of W22 and *Zman2* plants treated with 1 mM $CuSO_4$ for 48 h. Within individual analytes, asterisk (*) denote significant differences using Student t-tests (two-tailed distribution, unpaired) with all *P*s < 0.005 comparing between W22 and *Zman2* roots.

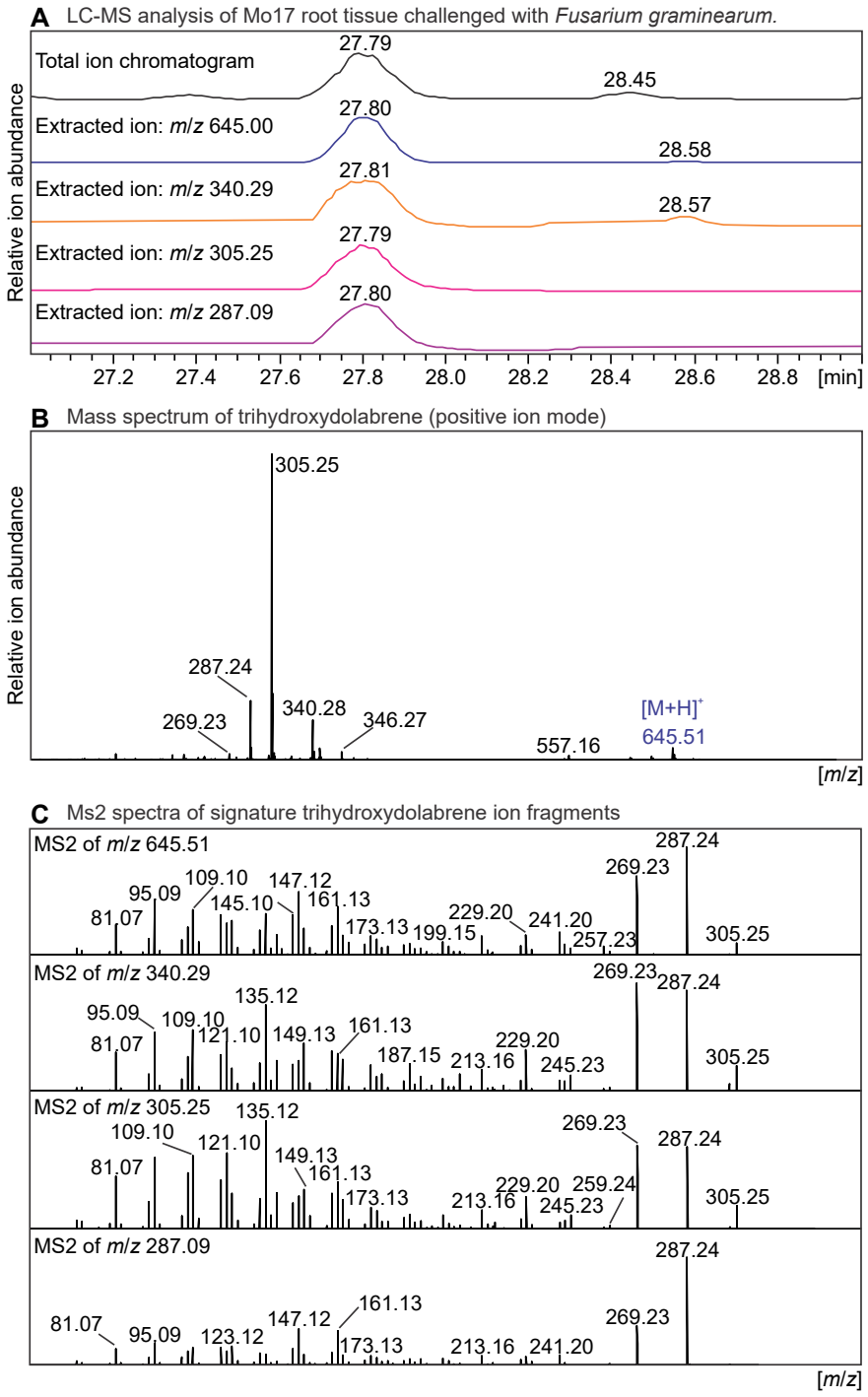

Supplemental Fig. S8: LC/MS-MS analysis of trihydroxydolabrene. [**A**] Total ion chromatogram and [**B**] mass spectrum of extracts from Mo17 root tissue challenged with live spores of fungal pathogen *Fusarium graminearum*, showing the compound with a parent ion of $[M+H]^+$ *m*/*z* 645.5. Analysis was performed using Q Exactive HF LC/MS-MS analysis with nano-spray ionization in positive mode. [**C**] MS/MS analyses of ion fragments of trihydroxydolabrene derived from "in source" decay. All tested ion fragments (*m*/*z* 340, *m*/*z* 305, *m*/*z* 287) show MS/MS spectra identical to epoxydolabranol (Fig. 4).

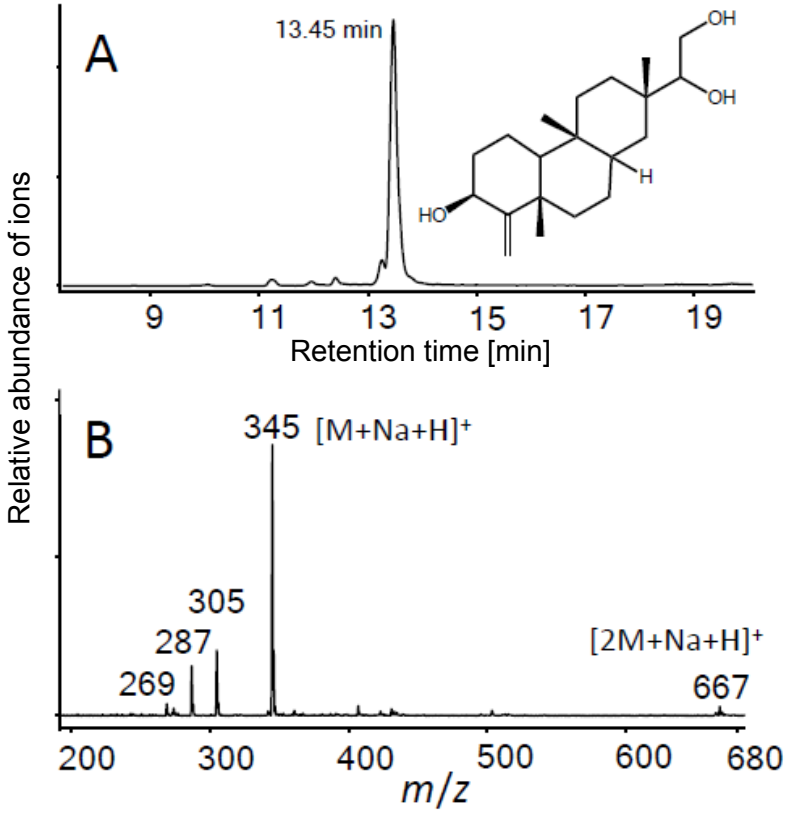

Figure S9. Routine analysis of 3β,15,16-trihydroxydolabrene. (**A**) Extracted ion chromatogram (EIC) of trihydroxydolabrene $[M+Na+H]^+$ *m*/*z* 345 acquired using C18 chromatography, a H_2O / MeOH gradient and positive electrospray ionization (ESI) coupled with an Agilent 6460 triple quadrapole mass spectrometer. (**B**) Ions associated with trihydroxydolabrene (exact mass = 322.25) include $[2M+Na+H]^+$, $[M+Na+H]^+$, $[M-H_2O+H]^+$, $[M-2H_2O+H]^+$ and $[M-3H_2O+H]^+$ corresponding to *m*/*z* 667, 345, 305, 287 and 269, respectively. Under no tested experimental conditions was a clear positive $[M+H]^+$ *m*/*z* 323 or negative $[M-H]^-$ *m*/*z* 321 parent ion detectable.

Supplemental Fig. S10: NMR elucidation of 3β,15,16-trihydroxydolabrene

(A) Proton chemical shifts ^{1}H-NMR (600 MHz, DMSO-d_6), δ (ppm): 1.66 (1H, m, H1a), 1.42 (1H, m, H1b), 1.83 (1H, m, H2a), 1.40 (1H, m, H2b), 4.13 (1H, m, H3), 4.50 (1H, bs, 3-OH), 1.61 (1H, m, H6a), 1.45 (1H, m, H6b), 1.41 (1H, m, H7a), 1.15 (1H, m, H7b), 1.17 (1H, m, H8), 0.81 (1H, m, H10), 1.52 (2H, m, H11), 1.51 (1H, m, H12a), 0.94 (1H, m, H12b), 1.15 (1H, m, H14a), 0.96 (1H, m, H14b), 3.92 (1H, m, H15), 3.98 (1H, t, J= 8.0, H16a), 3.87 (1H, m, H16b), 0.80 (3H, s, H17), 4.70 (1H, dd, J=4.5, 1.2, H18a), 4.63 (1H, dd, J=5.5, 1.2, H18b), 1.18 (3H, s, H19), 0.73 (3H, s, H_20).

Carbon chemical shifts and assignments based on HSQC and HMBC (600 MHz, DMSO-d_6), δ (ppm) were as follows: 16.6 (C1), 35.9 (C2), 73.0 (C3), 160.3 (C4), 40.5 (C5), 39.0 (C6), 25.7 (C7), 41.7 (C8), 37.5 (C9), 56.4 (C10), 34.7 (C11), 27.4 (C12), 37.1 (C13), 34.4 (C14), 83.5 (C15), 64.8 (C16), 18.9 (C17), 107.5 (C18), 23.4 (C19), 12.8 (C20).

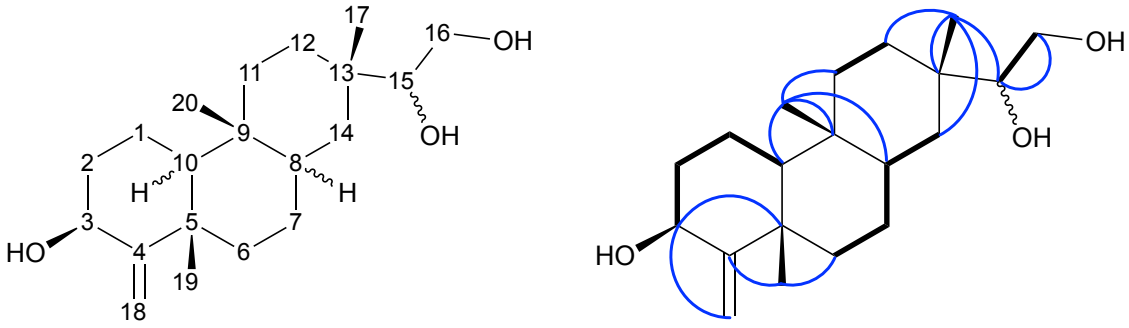

Supplemental Fig. S10, continued

^{1}H-NMR (600 MHz, DMSO-d_6)

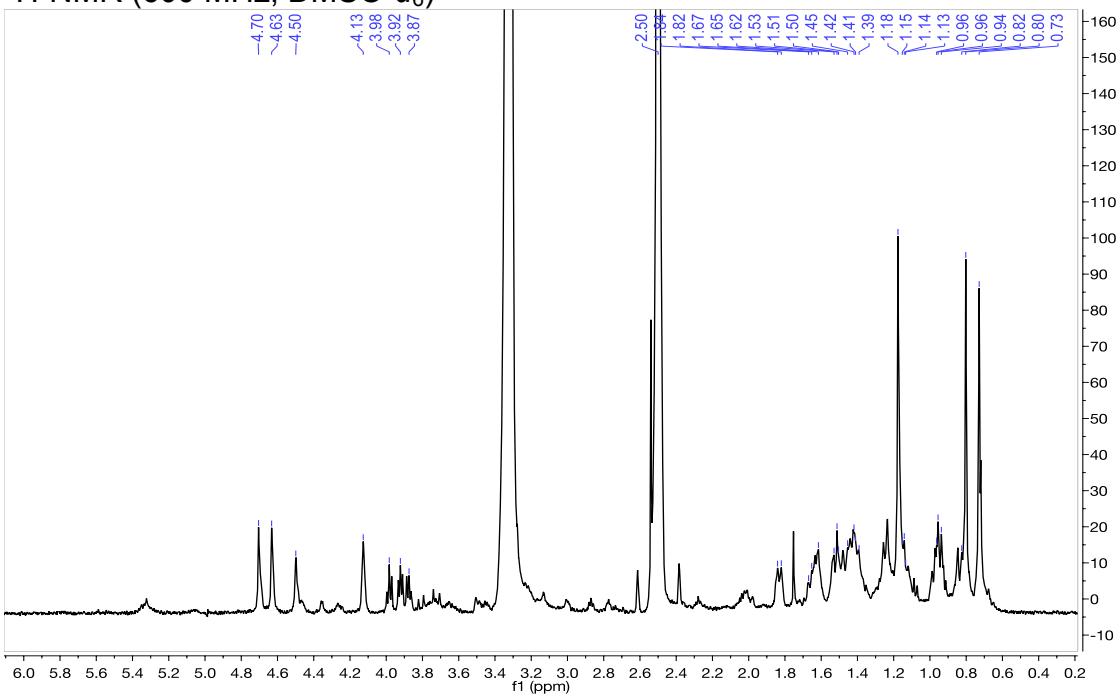

HSQC (600 MHz, DMSO-d_6)

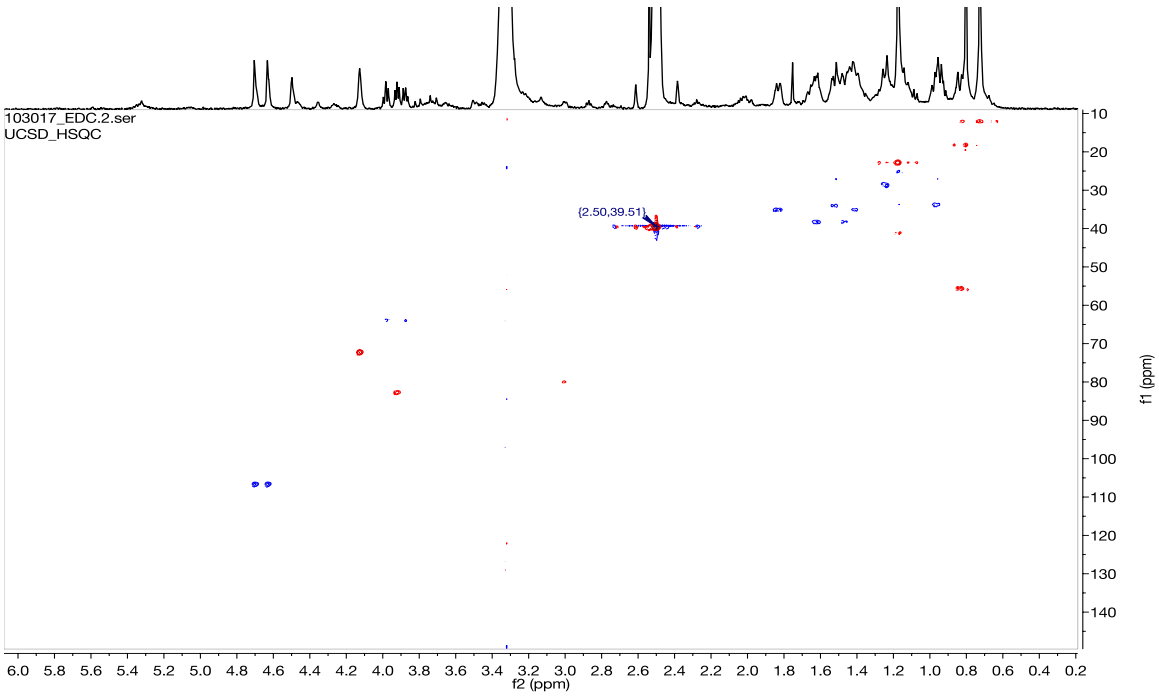

Supplemental Fig. S10, continued

COSY (600 MHz, DMSO-d_6)

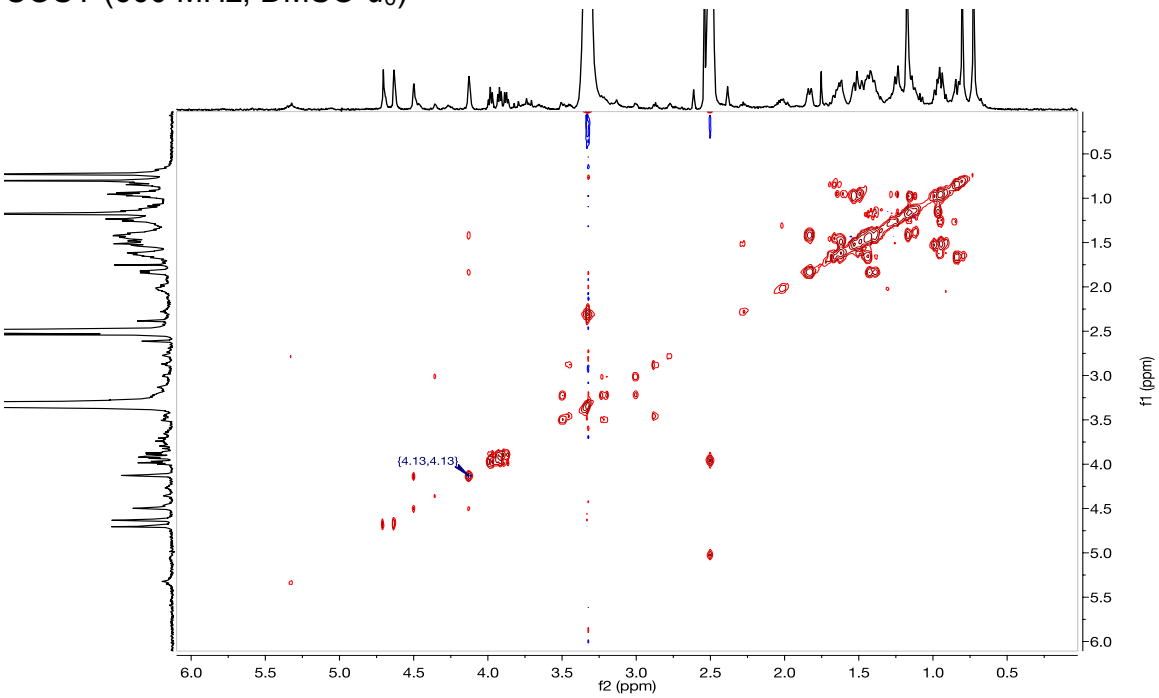

HMBC (600 MHz, DMSO-d_6)

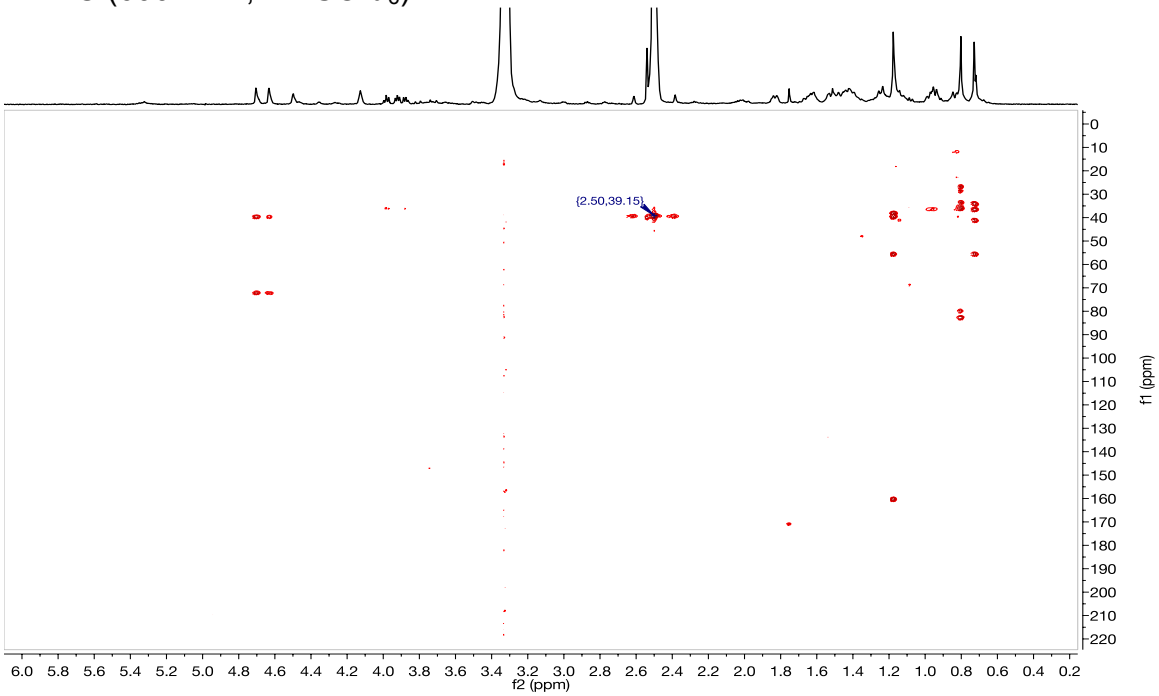

Supplemental Table S1: Oligonucleotides and genes used in this study.

Oligonucleotides			
Purpose	**Gene**	**Oligonucleotide**	**Sequence (5'-3')**
qPCR	ZmAn2	Forward	GACGCTCTACAGGATGCCTC
		Reverse	CCAGGAAATACGCTCGCAGA
	ZmKSL4	Forward	AAAGGGCTCTCTTTCGTCGG
		Reverse	AGCTTTACTTCCGGTGGTGG
	EF1-α	Forward	TGGGCCTACTGGTCTTACTACTGA
		Reverse	ACATACCCACGCTTCAGATCCT
	CYP71Z16	Forward	GACAAGCCACGAGTACCTCC
		Reverse	CATTAACCGGAGCAAAGCGG
E. coli expression	ZmKSL4	pET28b-F-Δ106	GAATTCGATGGGCGCCACCGACGACGGCTTA
		pET28b-R	GCGGCCGCAAGTTCCCTGACCCGCAGCGGAT
	ZmKSL4	pCOLA-DUET - F	GGA GAT ATA CATATGGGCGCCACCGACGAC
		pCOLA-DUET - R	GCCTAGGTTAATTAATCAAAGTTCCCTGACCCGC
	ZmFPPS3	pCOLA-DUET- F	GAAGGAGATATACATATGGCAACAGCCGAAGTTG
		pCOLA-DUET- R	CTTTACCAGACTCGAGTTATTTATCGCGTTTATAGA
	ZmTPS11	pCOLA-DUET-F	GAATTCGATGGCTGCCCCAACACTAACTA
		pCOLA-DUET-R	GAATTCTCACATGAGTACCGGCTTCACAT
	ZmCPR	pET-DUET1-F	CATGCCATGGCAGCACTGGAAGCAGTTCG
		pET-DUET1-R	CCCAAGCTTTTACCAAACATCACGCAGATAAC
	CYP71Z16	pET-DUET1-F	AGGAGATATACATATGGCCAAAAAAACCAGCAGC
		pET-DUET1-R	CTTTACCAGACTCGAGTTATGCATTAACCGGTGC
Yeast expression	CYP71Z18	pESC-Leu2D-F	GGAGAAAAAACCCCGGATCCATGGAGGACAAGGTGCTC
		pESC-Leu2D-R	GTACCAAGCTTACTCGAGTTAGGCATTAACCGGAGCAAAG
Codon-optimized synthetic gene sequences			
ZmFPPS3	ATGGCAACAGCCGAAGTTGTTGTTGCAAATGGTAGCGGTGGTGCAGATACCAAAACCGCATTTAAAGAGAT CTATAGCAAACTGAAACAAGAAATGCTGGAAGATCCGGCATTTGAATTTACCGATGAAAGCCTGCAATGGAT TGATCGTATGCTGGATTACAATGTTCTGGGTGGTAAATGTAATCGTGGTCTGAGCGTTGTTGATAGCTACAA AATTCTGAAAGGTGTTGACGTGCTGAGCAAAGAAGAAACCTTTCTGGCCTGTACCCTGGGTTGGTGTATTGA ATGGCTGCAAGCATATTTTCTGGTGCTGGATGATATTATGGATAACAGCCAGACCCGTCGTGGTCAGCCGT GTTGGTTTCGTGTTCCGCAGGTTGGTCTGATTGCAGTTAATGATGGTATTATTCTGCGCAACCATATCAGCC GTATTCTGCAACGTCATTTTAAAGGCAAACCGTATTATGTGGATATTATTGACCTGTTTAATGAAGTTGAGTTT AAAACCGCAAGCGGTCAGATGCTGGATCTGATTACCACCCATGAAGGTGAAAAAGATCTGACCAAATATAAC CTGACCGTGCATCGTCGTATTGTGCAGTATAAAACCGCCTATTATAGCTTTTATCTGCCGGTTGCATGTGCA CTGCTGCTGGCAGGCGAAAATCTGGAAAATTTTGTTGACGTGAAAAACATTCTGGTGGAAATGGGCACCTAT TTTCAGGTTCAGGATGATTATCTGGATTGCTTTGGTGATCCGGAATTTATTGGTAAAATTGGCACCGATATCG AAGATTACAAATGTAGCTGGCTGGTTGTTCAGGCACTGGAACGTGCAGCAGAAAATCAGAAAAGCATTCTGT TTGAGAACTATGGCAAAAGCGATCCGGCATGTGTTGCAAAAGTTAAAGATCTGTACAAAGAACTGAAACTGG AAGAGGTGTTTCATGAATATGAACGCGAGAGCTATAACAAACTGATTGCAGATATTGAAGCACAGCCGAGCA AAGCAGTTCAGACCGTTCTGAAAAGTTTTCTGCATAAAATCTATAAACGCGATAAATAA
ZmCPR2	ATGGCAGCACTGGAAGCAGTTCGTAGCTGGGCAGTTAGCGTTATTCCGCCTGAACTGGCAGCAGCAGCCG GTGGTGATCCGCTGGCTGCACTGGCAGCAACCGCAGCAGCACTGGTTGCAGGTCTGCTGATTCTGGCAGT TTGGTTTCGTAGCGGTGGTGGTGCACCGAGCAAACCGGTTGCAACACCGCTGCGTCCGCCTCCGGTTAAA GTTGATGCAGATGCAGATGTTGATGATGGTCGTAAACGTGTGACCATCTTTTTTGGCACCCAGACCGGCAC CGCAGAAGGTTTTGCAAAAAGCATGGCAGATGAAGCACGTGTGCGTTATGAAAAAGCCGTTTTTAAAGTTGT GGATCTGGATGATTATGCCCAAGAGGATGAAGAGTATGAAGAAAAACTGAAAAAAGAAACCGTGGCCCTGT TTTTTCTGGCAACCTATGGTGATGGTGAACCGACCGATAATGCAGCACGTTTCTATAAATGGTTTACCGAGG GCAAAGAAAAAGAGGTTTGGCTGAAAGATCTGAAATATGGCATTTTTGGTCTGGGCAATCGTCAGTATGAAC

	ACTTTAACAAAGTTGCCAAAGTGGTGGATGAACTGCTGGAAGAACAGGGTGGTAAACGTCTGGTTCCGGTT GGTCTGGGTGATGATGATCAGTGTATTGAAGATGATTTTACCGCCTGGAAAGAACTGGTTTGGCCTGAACTG GATCAGCTGCTGCGTGATGAAGATGATACCAATGGTGCAAGCACCCCGTATACCGCAGCAATTCCGGAATA TCGTGTTGTGTTTATTGATAAAAGCGACCTGAGCTTTCAGGATCGTAGCTGGTCACTGGCAAATGGCACCGG TGTTATTGATATTCATCATCCGTGTCGTGCAAATGTTGCAGTTCGTAAAGAACTGCATAAACCGGCAAGCGA TCGTAGCTGTATTCATCTGGAATTTGATATTAGCGGCACCAGCCTGGTTTATGAAACCGGTGATCATGTTGG TGTTTATGCCGAAAATAGCGTTGAAACCGTTGAAGAAGCAGAAAGCCTGCTGGATCTGAGTCCGGATACCG TTTTTAGCATTCATGCAGATGCCGAAGATGGTAGTCCGCGTAAAGGTGGTAGCAGCCTGGCACCGCCTTTT CCGAGCCCGTGTACCCTGCGTACCGCACTGCTGCGTTATGCAGATCTGCTGAATCCGCCTAAAAAAGCAGC ACTGCTGGCACTGGCAAGCCATGCAAGCGATCCGGCAGAAGCAGAACGTCTGCGTTTTCTGGCAAGTCCG GCAGGTAAAGATGAATATAGCCAGTGGATTACCGCAAGCCAGCGTAGCCTGCTGGAAGTTATGGCAGCATT TCCGAGCGCAAAACCGCCTCTGGGTGTTTTTTTTGCAGCAATTGCACCGCGTCTGCAGCCTCGTTATTATAG CATTAGCAGCAGCCCGAAAATGGCACCGAGCCGTATTCATGTTACCTGTGCACTGGTTTATGGTCCGAGCC CGACCGGTCGTATTCATCAGGGTGTTTGTAGCACCTGGATGAAAAATACCATTCCGCTGGAATATAGCGAAG AATGTAGCTGGGCACCGATTTTTGTTCGTCAGAGCAACTTTAAACTGCCTGCAGATCCGAGCACCCCGATTA TTATGATTGGTCCGGGTACAGGTCTGGCACCGTTTCGTGGTTTTCTGCAAGAACGTCTGGCACTGAAACAG AGCGGTGCAGAACTGGGCACCAGCATTCTGTTTTTTGGTTGTCGTAATCGCAACATGGATTACATCTATGAA GATGAACTGCAGACCTTTCTGGAAGAAGGTGCACTGAGCGAACTGATTGTTGCATTTAGCCGTGAAGGTCC GACCAAAGAATATGTTCAGCATAAAATGGTTGAGAAAGCCACCGAAATTTGGAACATTATTAGTCATGGTGG CTATCTGTATGTTTGCGGTGATGCAAAAGGTATGGCACGTGATGTTCATCGTATGCTGCATACCGTTGTTCA AGAACAGGGTAGCCTGGATAGCAGCAAAACCGAAAGCTATGTTAAAAGCCTGCAGATGGAAGGTCGTTATC TGCGTGATGTTTGGTAA
ZmCYP71Z16	ATGGCCAAAAAAACCAGCAGCAAAGGTAAACTGCCTCCGGGTCCGTGGACCCTGCCGCTGATTGGTAGCAT TCATCATCTGGTTAGCAGTCCGCTGCCGTATCGTGCAATGCGTGAACTGGCACATAAACATGGTCCGCTGA TGATGCTGTGGCTGGGTGAAGTTCCGACCCTGGTTGTTAGCTCACCGGAAGCAGCACAGGCAATTACCAAA ACCCATGATGTTACCTTTGCAGATCGTCACATGAATAGCACCGTTGATATTCTGACCTTTAACGGCAACGATA TTGTGTTTGGCACCTATGGTGAACAGTGGCGTCAGCTGCGTAAACTGAGCGTTCTGGAACTGCTGAGCGTT GCACGTGTTCAGAGCTTTCAGCGTATTCGTGAAGAAGAGGTTGCACGTTTTATGCGTAATCTGGCAGCAAGT GCCGGTGCCGGTGCAACCGTTGATCTGAGCAAAATGATTAGCAGCTTTATCAACGATACCTTTGTGCGTGAA AGCATTGGTAGCCGTTGTAAACATCAGGATGAATATCTGGATGCACTGCATACCGGTATTCGTGTTGCAGCA GAACTGAGCGTTGCCAACCTGTTTCCGAGCAGCCGTCTGCTGCAGAGCCTGAGCACCGCACGTCGTAAAG CAGTTGCAGCACGTGATGAAATGGCACGTATTCTGGGTCAGATTATTCGTGAAACCAAAGAAGCAATGGATT GGGGAGATAAAGCAAGCAATGAAAGCATGATTAGCGTTCTGCTGCGTCTGCAGAAAGAAGCAGGTCTGCCG ATTGAACTGACCGATGATATTGTTATGGCACTGATGTTTGACCTGTTTGGTGCAGGTAGCGATACCAGCAGC ACCACCCTGACCTGGTGTATGACCGAAATGATTCGTTATCCGGCAACAATGGCAAAAGCACAGGCCGAAGT TCGTGAAGCATTTAAAGGTAAAACCACCATCACCGAAGATGATCTGAGCCGTGCAAATCTGAGCTATCTGAA ACTGGTTGTTAAAGAAGCACTGCGTCTGCATTGTCCGGTTCCGCTGCTGATTCCGCGTAAATGTCGTGAAAC CTGTCAGATTATGGGTTATGATATTCCGAAAGATACCTGCGTTCTGGTTAATGTTTGGGCAATTTGTCGTGAT AGCCGTTATTGGGAAGATGCCGATGAATTTAAACCGGAACGTTTTGAAAATAGCAGCCTGGATTATAAAGGC ACCAGCCATGAATATCTGCCGTTTGGTAGCGGTCGTCGTATGTGTCCGGGTGGTAATCTGGGTGTTGCAAA TATGGAACTGGCACTGGCAAGCCTGCTGTATCATTTTGATTGGAAACTGCCGAGCGGTCAAGAACCGAAAG ATGTTGATGTTTGGGAAGCAGCAGGTCTGGTTGGTCGTAAAAATGCCGGTCTGGTTCTGCATCCGGTTAGC CGTTTTGCACCGGTTAATGCATAA

Supplemental Table 2: Protein sequences used in phylogenetic analyses.

Name	Organism, function	UniProtKB/*Genbank* ID
Diterpene synthases		
HvKSL1	*Hordeum vulgare ent*-kaurene synthase 1	AAT49066
OsKS1	*Oryza sativa ent*-kaurene synthase	NP_001053841
OsKSL4	*Oryza sativa syn*-pimara-7,15-ene synthase	NP_001052175
OsKSL5	*Oryza sativa ent*-iso-kaurene synthase	NP_001047190
OsKSL6	*Oryza sativa ent*-iso-kaurene synthase	ABH10733
OsKSL7	*Oryza sativa ent*-cassadiene synthase	NP_001047186
OsKSL8	*Oryza sativa syn*-stemarene synthase	NP_001067887
OsKSL10	*Oryza sativa ent*-sandaracopimaradiene synthase	NP_001066799
OsKSL11	*Oryza sativa syn*-stemodene synthase	Q1AHB2
PgEKS	*Picea glauca ent*-kaurene synthase	D2XEB3
PpCPSKS	*Physcomitrella patens ent*-CPP/*ent*-kaurene synthase	A5A8G0
TaKSL1	*Triticum aestivum* isopimara-7,15-ene synthase	AB597957
TaKSL2	*Triticum aestivum ent*-pimara-8(14),15-ene synthase	AB597958
TaKSL3	*Triticum aestivum* uncharacterized	AB597959
TaKSL4	*Triticum aestivum* pimara-8,15-ene synthase	AB597960
TaKSL5	*Triticum aestivum ent*-kaurene/beyerane synthase	AB597961
TaKSL6	*Triticum aestivum ent*-kaurene synthase	AB597962
ZmKSL1	*Zea mays* kaurene-synthase-like 1	AFW61735
ZmKSL2	*Zea mays* kaurene-synthase-like 2	DAA54948
ZmKSL3	*Zea mays ent*-kaurene synthase	DAA36069
ZmKSL4	*Zea mays* kaurene-synthase-like	DAA49845
ZmKSL5	*Zea mays ent*-kaurene synthase	NP_001141888
ZmTPS1	*Zea mays ent*-kaurene synthase	AAO18435
Cytochrome P450 monoxygenases		
AtrCYP71	*Amborella trichopoda* putative CYP71-like	ERN15844
CYP71C1	*Zea mays* 3-hydroxyindolin-2-one monooxygenase	Q43250
CYP71C2	*Zea mays* indolin-2-one monooxygenase	Q43255
CYP71C3	*Zea mays* uncharacterized	P93703
CYP71Z7	*Oryza sativa ent*-cassadiene C2-hydroxylase	Q6YV88
CYP71C4	*Zea mays* indole-2-monooxygenase	Q43257
CYP71Z1	*Oryza sativa* uncharacterized	XP_015634516
CYP71Z6	*Oryza sativa ent*-isokaurene C2-hydroxylase	A3A871
CYP71Z16	*Zea mays* dolabradiene oxygenase	GRMZM2G067591
CYP71Z18	*Zea mays* (*S*)-β-macrocarpene oxygenase	NP_001141366
CYP71AV1	*Artemisia annua* amorpha-4,11-diene 12-monooxygenase	Q1PS23
CYP71AV8	*Cichorium intybus* valencene oxidase	E1B2Z9
CYP71BL1	*Helianthus annuus* germacrene hydroxylase	F8S1H3
CYP71D12	*Catharanthus roseus* tabersonine 16-hydroxylase	P98183
CYP71A10	*Glycine max* phenylurea metabolism	O48918
CYP71D55	*Hyoscyamus muticus* premnaspirodiene oxygenase	A6YIH8
CYP71D13	*Mentha piperita* 4*S*-limonene hydroxylase	Q9XHE7
CYP71D18	*Mentha spicata* 4*S*-limonene hydroxylase	Q9XHE8
CYP71D16	*Nicotiana tabacum* uncharacterized	AAD47832
CYP71D20	*Nicotiana tabacum* 5-epiaristolochene-1,3-dihydroxylase	Q94FM7
PfCYP71	*Perilla frutescens* (-)-limonene-7-hydroxylase	D4N1M3
CYP71BA1	*Zingiber zerumbet* alpha-humulene 10-hydroxylase	E3W9C4